University of Texas Rio Grande Valley

ScholarWorks @ UTRGV

Mechanical Engineering Faculty Publications and Presentations

College of Engineering and Computer Science

11-1-2020

# Centrifugally spun mats based on biopolyesters/hydroxyapatite and their potential as bone scaffolds

Victoria Padilla-Gainza

Heriberto Rodríguez-Tobías

Graciela Morales

Eduardo Saucedo

Karen Lozano

*See next page for additional authors*

Follow this and additional works at: https://scholarworks.utrgv.edu/me_fac

 Part of the Mechanical Engineering Commons

## Authors

Victoria Padilla-Gainza; Heriberto Rodríguez-Tobías; Graciela Morales; Eduardo Saucedo; Karen Lozano; Vanessa Montaño-Machado,; and Diego Mantovani

Check for updates

Padilla Gainza Victoria Maria (Orcid ID: 0000-0002-4676-1337)

# Centrifugally spun mats based on biopolyesters/hydroxyapatite and their potential as bone scaffolds

V. Padilla-Gainza[1,2*], H. Rodríguez-Tobías[1], G. Morales[1*], E. Saucedo-Salazar[1], K. Lozano[2], V. Montaño-Machado[3] and D. Mantovani[3]

[1] Centro de Investigación en Química Aplicada, Blvd. Enrique Reyna 140, Saltillo, CP 25294, Coah., México
[2] University of Texas Rio Grande Valley, 1201 West University Drive, Edinburg, TX 78539, USA
[3] Laboratory for Biomaterials and Bioengineering (CRC-I), Dept. of Min-Met-Materials Eng. & Regenerative Medicine, CHU de Quebec Research Center, Laval University, Quebec, Canada

**Graciela.morales@ciqa.edu.mx, victoria.padilla@utrgv.edu**

Victoria Maria Padilla Gainza
Affiliation: Centro de Investigación en Química Aplicada, Blvd. Enrique Reyna 140, Saltillo, CP 25294, Coah., Mexico.
ORCID: 0000-0002-4676-1337
e-mail: viquipadilla@gmail.com/ victoria.padilla@utrgv.edu

Heriberto Rodríguez Tobías
Affiliation: Centro de Investigación en Química Aplicada, Blvd. Enrique Reyna 140, Saltillo, CP 25294, Coah., Mexico.
ORCID: 0000-0001-9608-5843
e-mail: lcq.heriberto.rodriguez@gmail.com

Graciela Morales
Affiliation: Centro de Investigación en Química Aplicada, Blvd. Enrique Reyna 140, Saltillo, CP 25294, Coah., Mexico.
ORCID: 0000-0003-0714-4325
e-mail: graciela.morales@ciqa.edu.mx

Esmeralda Monserrat Saucedo Salazar
Affiliation: Centro de Investigación en Química Aplicada, Blvd. Enrique Reyna 140, Saltillo, CP 25294, Coah., Mexico.
ORCID: 0000-0002-9985-1897
e-mail: esmeralda.saucedo@ciqa.edu.mx

Karen Lozano
Affiliation: University of Texas Rio Grande Valley, 1201 West University Drive, Edinburg, TX 78539, USA.
ORCID: 0000-0002-6676-8632
e-mail: karen.lozano@utrgv.edu

Vanessa Montaño Machado
Affiliation: Laboratory for Biomaterials and Bioengineering (CRC-I), Dept. of Min-Met-Materials Eng. & Regenerative Medicine, CHU de Quebec Research Center, Laval University, Quebec, Canada
ORCID: 0000-0002-7015-588X
e-mail: vmontano24@gmail.com

Diego Mantovani

This is the author manuscript accepted for publication and has undergone full peer review but has not been through the copyediting, typesetting, pagination and proofreading process, which may lead to differences between this version and the Version of Record. Please cite this article as doi: 10.1002/app.50139

This article is protected by copyright. All rights reserved.

Author Manuscript

10974628, 2021, 14, Downloaded from https://onlinelibrary.wiley.com/doi/10.1002/app.50139 by The University Of Texas Rio Grande Valley, Wiley Online Library on [19/12/2022]. See the Terms and Conditions (https://onlinelibrary.wiley.com/terms-and-conditions) on Wiley Online Library for rules of use; OA articles are governed by the applicable Creative Commons License

Affiliation: Laboratory for Biomaterials and Bioengineering (CRC-I), Dept. of Min-Met-Materials Eng. & Regenerative Medicine, CHU de Quebec Research Center, Laval University, Quebec, Canada
ORCID: 0000-0001-9672-895X
e-mail: diego.mantovani@gmn.ulaval.ca

# Centrifugally spun mats based on biopolyesters/hydroxyapatite and their potential as bone scaffolds

V. Padilla-Gainza[1,2*], H. Rodríguez-Tobías[1], G. Morales[1*], E. Saucedo-Salazar[1], K. Lozano[2], V. Montaño-Machado[3] and D. Mantovani[3]

[1] Centro de Investigación en Química Aplicada, Blvd. Enrique Reyna 140, Saltillo, CP 25294, Coah., México
[2] University of Texas Rio Grande Valley, 1201 West University Drive, Edinburg, TX 78539, USA
[3] Laboratory for Biomaterials and Bioengineering (CRC-I), Dept. of Min-Met-Materials Eng. & Regenerative Medicine, CHU de Quebec Research Center, Laval University, Quebec, Canada

**Graciela.morales@ciqa.edu.mx, victoria.padilla@utrgv.edu**

## Abstract

This work studied the potential of centrifugal spinning for the production of fibrous materials based on poly(D,L-lactic acid) (PDLLA) and poly(3-hydroxybutyrate) (PHB) with hydroxyapatite nanoparticles (n-Hap). The influence of n-Hap concentration (5, 10 and 15 wt %) and spinneret angular speed on the final fiber morphology were analyzed. Further experimental evaluations were implemented to determine the effect of n-Hap on the thermal and mechanical performance. The optimum parameters that show a balance among high yield production of homogeneous fibers with the smallest fiber average diameter were found to be at 5 wt % of n-Hap processed at 7000 rpm for PDLLA, and 5, 10 and 15 wt % of n-Hap at 6000 rpm for PHB. The thermal stability, for both systems, was not significantly affected. The mechanical performance of PHB systems was improved with the addition of n-Hap. Osteoblast cell viability tests depicted a favorable cell response on the PDLLA systems.

## 1. Introduction

Hydroxyapatite nanoparticle (n-Hap) is a ceramic material mainly used in applications related to bone tissue, due to its resemblance to bone in structure and composition. Several recent studies reported that n-Hap contributes to important biological processes for bone tissue regeneration,



This article is protected by copyright. All rights reserved.

Author Manuscript

10974628, 2021, 14, Downloaded from https://onlinelibrary.wiley.com/doi/10.1002/app.50139 by The University Of Texas Rio Grande Valley, Wiley Online Library on [19/12/2022]. See the Terms and Conditions (https://onlinelibrary.wiley.com/terms-and-conditions) on Wiley Online Library for rules of use; OA articles are governed by the applicable Creative Commons License

such as osteoconduction[1] (bone growth at the superficial level), osteoinduction[2] (pluripotent cells are stimulated to develop bone-forming cells, a process that induces osteogenesis) and osseointegration[3] (stable anchorage of an implant, obtained by direct contact between the bone tissue and the implant). The major limitation in the use of n-Hap-based materials as bone implants is their poor mechanical behavior, increasing their fragility when they are manufactured in the form of scaffolds with high porosity to mimic the bone structure. Therefore, these ceramic compounds are commonly used as fillers or coatings in polymeric matrices.[4]

The design of polymeric scaffolds with n-Hap has been widely explored due to their effective regenerative characteristics, mainly those based on synthetic and natural biopolymers.[5] In the biomedical area, the approach has been tilted in the production of polymer fiber scaffolds as they are systems that provide a structural morphology similar to the extracellular matrix of various tissues within the human body. The interest in this type of hybrid materials has promoted their study with different line cells, obtaining promising results for applications in tissue engineering.[1,6–9]

Several research teams have worked on the design of fibrous materials based on PHB/Hap produced by electrospinning. Ramier *et al.*[7] reported changes in the roughness of the fiber which resulted in improvements in the mechanical properties (Young's module, tensile strength), and increased adhesion and differentiation of human stromal mesenchymal cells (hMSc). Sadat-Shojai *et al.*[6] results provided information that n-Hap have not a cytotoxic effect on mouse pre-osteoblast cells (MC3T3-E1) under *in vitro* conditions, thus suggesting further use for *in vivo* evaluation.

Poly(L-lactic acid) (PLLA) has also been explored for the design of n-Hap hybrid nanofiber membranes through the same technique than PHB/Hap. Morelli *et al.*[1] reported the influence of n-Hap on surface morphology and average fiber diameter and observed a decrease in mechanical performance (Young's modulus, tensile strength) by increasing the concentration of n-Hap to 50 wt %. On the other hand, Novotra *et al.*[8] designed polymeric fibers containing 5 and 15 wt % of n-Hap, with similar tensile mechanical performance (stiffness and % of elongation at break);



This article is protected by copyright. All rights reserved.

Author Manuscript

10974628, 2021, 14, Downloaded from https://onlinelibrary.wiley.com/doi/10.1002/app.50139 by The University Of Texas Rio Grande Valley, Wiley Online Library on [19/12/2022]. See the Terms and Conditions (https://onlinelibrary.wiley.com/terms-and-conditions) on Wiley Online Library for rules of use; OA articles are governed by the applicable Creative Commons License

furthermore, *in vitro* tests demonstrated good support for adhesion, growth and osteogenic differentiation. Recently, Sánchez-Arevalo *et al.*[9] observed changes in the surface morphology and diameter of PLLA fibers obtained at concentrations of 2, 4 and 6 wt % of n-Hap; and found that at a concentration of 2 wt % there was a decrease in macro and micro tensile mechanical properties (Young's modulus).

Electrospinning has been the preferred method to produce the needed nanofiber membranes.[10] However, this technique has certain limitations such as the need to use solvents with specific dielectric properties, high energy cost due to the required high voltage, and for lab scale single-needle electrospinning systems, low production rates (typically 10-100 $mg \cdot h^{-1}$).[11] Alternative technologies have been developed with the purpose to overcome some of the electrospinning limitations. One of these technologies is the centrifugal spinning, a competitive option given its high production rate (50-100 $g \cdot h^{-1}$)[12–14] and lower operational cost since there is no need for electric fields and can easily be used for solvents or melts (further decreasing cost).

In this work, the process conditions for obtaining hybrid materials based on homogeneous PDLLA and PHB fibers with n-Hap are reported using the centrifugal spinning technique, Forcespinning®. In addition, an analysis of the influence of such nanoparticles on the morphological characteristics of the obtained fibers was established. Finally, aspects related to the influence of n-Hap on the thermal and mechanical performance as well as the interaction of the design materials with osteoblast cells were addressed to assess their potential application as bone scaffolds.

## 2. Experimental Methodology

### 2.1. Materials and reagents

Poly(D, L-lactic acid) (PDLLA) provided by NatureWorks LLC (Ingeo 6362D) with $M_w$=160 kg $mol^{-1}$ and Đ = 1.646, and poly(3-hydroxybutyrate) (PHB) supplied by Goodfellow with $M_w$= 381 kg $mol^{-1}$; Đ = 3.53, were used as the polymer matrices. Chloroform, ACS grade, was purchased



This article is protected by copyright. All rights reserved.

Author Manuscript

10974628, 2021, 14, Downloaded from https://onlinelibrary.wiley.com/doi/10.1002/app.50139 by The University Of Texas Rio Grande Valley, Wiley Online Library on [19/12/2022]. See the Terms and Conditions (https://onlinelibrary.wiley.com/terms-and-conditions) on Wiley Online Library for rules of use; OA articles are governed by the applicable Creative Commons License

from Fisher Scientific. Hydroxyapatite (Hap), $D_p \leq 200$ nm and 97% of purity, was obtained from Sigma-Aldrich.

### 2.2. Preparation of precursor solutions

Several dispersions with different n-Hap concentrations were prepared using chloroform as the liquid medium. The n-Hap was dispersed using an ultrasound bath (Cole-Parmer 8891) for 50 min. Once the dispersion process was finished, the polymer was added to the system in an amount corresponding to the established concentration. In the case of PDLLA, the solution was carried out under constant stirring for 22 h at room temperature, while for PHB the system was maintained at a temperature of 55 °C, during a stirring time which varied between 12-16 h.

The viscosities of the biopolyester solutions were determined using an Anton Paar rheometer, physical model MCR 301 with a cone-plate configuration (diameter 50 mm, angle of 2 ° and gap of 0.205) at 25 °C.

### 2.3. Centrifugal spinning process

The prepared solutions were subjected to a centrifugal spinning process in a Cyclone™ L-1000M (FiberRio Technology, Corp.), which consist of a cylindrical spinneret with two nozzles equipped with regular beveled needles (30-gauge length, Becton, Dickinson and Company) and 8 collectors in the form of metal bars arranged around the spinneret at a distance of 15 cm from the nozzles. For each run, 2 mL of polymer solution were added to the spinneret, and fiber spinning was carried out for 5 min at a temperature of 24.1 °C ± 1.5 °C with a relative humidity of 54.3% ± 8.7%. It is important to mention that the fiber characterization in the optimization stage was determined from the fibers collected from a single run (5 min). Once proper parameters were established, the resultant mats were obtained by the collection of 7-runs (5 min each). The fibers were placed in a



This article is protected by copyright. All rights reserved.

Author Manuscript

10974628, 2021, 14, Downloaded from https://onlinelibrary.wiley.com/doi/10.1002/app.50139 by The University Of Texas Rio Grande Valley, Wiley Online Library on [19/12/2022]. See the Terms and Conditions (https://onlinelibrary.wiley.com/terms-and-conditions) on Wiley Online Library for rules of use; OA articles are governed by the applicable Creative Commons License

vacuum oven at 30 °C for 24 h, to remove any residual solvent. Finally, the fibers were stored in plastic bags in the presence of a desiccant for moisture control.

### 2.4. Experimental design

Table 1 presents the precursor solution concentration and intervals of angular speed (ω) used in the production of the fiber-based mats.

**Table 1.-** Experimental conditions used during the centrifugal spinning process.

| | $C_p$ (wt %) | ω (rpm) | $C_{Hap}$ (wt %) | Identification |
|---|---|---|---|---|
| **PDLLA** | 10 | 6000-9000 | 5, 10, 15 | PDLLA-Hap 5% |
| | | | | PDLLA-Hap 10% |
| | | | | PDLLA-Hap 15% |
| **PHB** | 9 | | | PHB-Hap 5% |
| | | | | PHB-Hap 10% |
| | | | | PHB-Hap 15% |

*ω= angular speed, $C_p$ = polymer concentration and $C_{Hap}$ = Hap concentration

For the selection of the optimum ω, resultant fiber morphology, fiber diameter, and ultimate yield were considered. The yield/output of the process ($\eta_p$) was estimated by Equation 1.

$$\eta_P = \frac{M_{mf}}{ST} x100 \quad (1)$$

where $M_{mf}$ and $ST$ are the grams of fibers collected per run (5 min) and the total solids (polymer + NPs) contained in 2 mL of polymer solution, respectively.

### 2.5. Fibrous material characterization

The morphological analysis was carried out using a scanning electron microscope (Carl Zeiss, SigmaVP). The images obtained were analyzed with the Image J software (v. 1.48) to estimate



This article is protected by copyright. All rights reserved.

Author Manuscript

10974628, 2021, 14, Downloaded from https://onlinelibrary.wiley.com/doi/10.1002/app.50139 by The University Of Texas Rio Grande Valley, Wiley Online Library on [19/12/2022]. See the Terms and Conditions (https://onlinelibrary.wiley.com/terms-and-conditions) on Wiley Online Library for rules of use; OA articles are governed by the applicable Creative Commons License

Author Manuscript

average fiber diameters ($\overline{D_f}$) and average pore size (interfibrillar spaces). Diameter distributions were obtained by measuring 100 fibers (20 fibers per micrograph) with three measurements per fiber, making a total of 300 measurements per sample. Obtained data was represented by means of box-bars charts, where the boxes reflect 50% of the population of values that located between quartile 1 ($Q_1$ = 25% of the population) and 3 ($Q_3$ = 75% of the population) and the bars represent the amplitude of the distribution according to the most probable values or those that appear more frequently.

The distribution and dispersion of the n-Hap within the fibers were determined using energy dispersive X-ray spectroscopy (EDS, EDAX Octane Super) and transmission electron microscopy (FEI, Titan 80-300).

For the calculation of the scaffold's porosity, an adjustment of the equation reported by Wang[15] was used (Equation 2).

$$\emptyset = \left(1 - \frac{m}{Z*A*H*\rho}\right)*100 \qquad (2)$$

Where m, Z, A, H and ρ are the mass, thickness, width, and length of the scaffold and the density of the polymer with n-Hap in the corresponding case, respectively.

The thermal properties were evaluated through thermogravimetric analysis (TGA) (TA Instruments, Q400) and differential scanning calorimetry (DSC) (TA Instruments, Q200). To perform the TGA, the samples were heated from 30 °C to 600 °C under a nitrogen atmosphere, at a heating rate of 10 °C·min$^{-1}$. Regarding the DSC, the heating was carried out from -70 to 200 °C at a rate of 10 °C·min$^{-1}$, the samples were isothermally maintained at 200 °C for 2 minutes and then cooled down at the same rate to -70 °C. A second heating cycle under the same conditions was conducted. The crystallinity of the systems manufactured with PHB was determined using Equation 3:[16]



This article is protected by copyright. All rights reserved.

10974628, 2021, 14, Downloaded from https://onlinelibrary.wiley.com/doi/10.1002/app.50139 by The University Of Texas Rio Grande Valley, Wiley Online Library on [19/12/2022]. See the Terms and Conditions (https://onlinelibrary.wiley.com/terms-and-conditions) on Wiley Online Library for rules of use; OA articles are governed by the applicable Creative Commons License

$$X_c = \frac{\Delta H_m}{\Delta H_m^{\circ} \times X_{PHB}} \times 100 \quad (3)$$

Where $\Delta H_m$ and $\Delta H_m^{\circ}$ are the melting enthalpies of the PHB sample and a 100% crystalline PHB respectively, being $\Delta H_m^{\circ}$ = 146 J·g$^{-1}$.[17] The $X_{PHB}$ is the PHB weight fraction in the sample.

The mechanical properties of the fibrous materials were determined by tensile tests using the universal testing machine (Tinius-Olsen, H10KS). The tensile testing was made using the paper frame method.[18,19] To this end, test pieces of 30 mm long and 3 mm wide were cut and conditioned for 24 h at room temperature (23-25 °C). The tensile tests were carried out at a deformation speed of 2 mm·min$^{-1}$ with a clamp separation of 27.5 mm, using a 50 N load cell (5 repetitions).

### 2.6. Cell viability test

Saos-2 (osteoblast like) cells were cultured in a flask with McCoy's culture media (Sigma, M4892-10X1L) containing 2.2g·L$^{-1}$ of $NaHCO_3$, 15% of fetal bovine serum (Fisher Thermo Scientific, SH30396.03) and 1% of Penicillin-Streptomycin (Gibco, 15140–122). Culture media was changed after 24 h and then each 48 h until cell confluence. Third to fifth generation of cells were used to evaluate their interaction with the PDLLA or PHB surfaces. Cells were removed from the culture plates by rinsing in PBS and incubating in a trypsin solution. After trypsin inactivation, the cells were centrifuged for 5 min at 1200 rpm. The resulting pellet was resuspended in complete medium. 30000 cells in McCoy's culture media containing serum and penicillin-streptomycin were deposited on PDLLA and PHB samples of 1x1 cm, previously sterilized with UV light for 20 min, and incubated at 37 °C. After adhesion for the specified time, cells were rinsed with PBS in order to eliminate all the rests of culture medium. 300 mL of solution of resazurin (Aldrich, 1001140130) on culture medium (1:10) was then added to the samples and was allowed to react for 4 h. 150 µl were taken from each sample and fluorescence was measured at 570 nm using a spectrophotometer Elisa reader (BioRad mod.450).



This article is protected by copyright. All rights reserved.

Author Manuscript

10974628, 2021, 14, Downloaded from https://onlinelibrary.wiley.com/doi/10.1002/app.50139 by The University Of Texas Rio Grande Valley, Wiley Online Library on [19/12/2022]. See the Terms and Conditions (https://onlinelibrary.wiley.com/terms-and-conditions) on Wiley Online Library for rules of use; OA articles are governed by the applicable Creative Commons License

Author Manuscript

## 3. Results and Discussion

### 3.1. Effect of n-Hap concentration on fiber formation

An optimization study was conducted for the PDLLA based systems using concentrations of n-Hap at 5, 10 and 15 wt % in an interval of ω between 5000 and 8000 rpm, in order to evaluate the influence of n-Hap on fiber formation (Figure S1, *Supplementary Information*). It was evidenced that the higher n-Hap concentration promotes the formation of defects within the fibers. This effect occurs more pronouncedly at 5000 rpm, whereas at a concentration of 15 wt % of n-Hap fibers exhibited a high level of ovoid defects. This fact produced a decrease in the amount of collectible material, affecting the process yield ($\eta_p$) ($\eta_p$ < 20%). The opposite occurred as ω increased, homogeneous fibers at a concentration of 5 wt % in the range of 7000 to 8000 rpm were obtained. In view of the difficulties presented with the incorporation of n-Hap, the criterion for selecting the best conditions was based on the fiber homogeneity and fiber yield. Therefore, the system obtained at 5 wt % of n-Hap and 7000 rpm was selected ($\eta_p$ = 67%, $Q_1$-$Q_3$ = 0.44-1.70 µm, $\overline{D_f}$ = 1.29 ± 1.14 µm) as one of the most suitable.

Figure 1 shows the influence of n-Hap concentration on fiber morphology and $\overline{D_f}$, it is compared to the system without n-Hap. Under the selected conditions, the incorporation of n-Hap did not have a pronounced effect on the material appearance, presenting a homogeneous morphology and a similar surface porosity. Regarding the $\overline{D_f}$ values, the effect was more pronounced, at 5 wt % of n-Hap where a wider dispersion (0.10 to 3.58 µm) and an increase of $\overline{D_f}$ from 1.03 to 1.29 µm was observed. This behavior was also observed by Morelli *et al.*[1] and Sanchez *et al.*[9] The increase in the amplitude of the fiber diameter distribution could be related to the n-Hap particle diameter distribution. Although $\overline{D_p}$ is around 44 nm, there is a small population with diameters ranging between 100 and 350 nm (Figure S2d, *Supplementary Information*), which could lead to the formation of thicker fibers.



This article is protected by copyright. All rights reserved.

10974628, 2021, 14, Downloaded from https://onlinelibrary.wiley.com/doi/10.1002/app.50139 by The University Of Texas Rio Grande Valley, Wiley Online Library on [19/12/2022]. See the Terms and Conditions (https://onlinelibrary.wiley.com/terms-and-conditions) on Wiley Online Library for rules of use; OA articles are governed by the applicable Creative Commons License

The apparent viscosity of the polymer solutions was evaluated as a function of the shear rate with and without n-Hap (Figure 1d). As it can be observed, at 5wt % of n-Hap a decrease in viscosity was observed compared to the system without n-Hap.

The interaction among the Hap and PLA has been reported in several studies such as Neuendorf *et al.*[20] where they performed surface tension measurements to determine the work of adhesion between Hap and all stereochemical forms of PLA (-DL, -D and -L), they found that the adhesion strength between Hap and PDLLA (-DL) is 20% greater in comparison with the other stereochemical forms.The obtained value, 63 J/m$^2$, can be associated with physical bonding across the organic/inorganic interface. On the other hand, Zhou *et al.*[21] reported the presence of hydrogen bond between the C = O group of the PDLLA and the OH groups present in the Hap. These studies, and taking into consideration that the size of the NPs (44.4 ± 36.3nm) is in the order of the radius of gyration of the polymer (30-40 nm),[22] provide information to suggest that the incorporation of the n-Hap produced a conformational change in the polymer chains (the chains are adsorbed on the surface of the particles) leading to a lower proportion of free polymer chains interacting with the solvent.[23] This phenomenon could then explain the observed decrease in the viscosity for samples containing 5 wt % of n-Hap. Additionally, this particle-polymer interaction provides a faster rate of solvent evaporation during the fiber formation process therefore leading to larger fiber diameters.

In the case of PHB, the interval of ω selected for the optimization study was 6000-9000 rpm at the same n-Hap concentrations evaluated for the PDLLA systems (Figure S3, *Supplementary Information*). In contrast to the latter, the formation of mostly homogeneous fibers was presented in the selected interval. Considering the obtained results, it could be established that the best angular speed for the manufacture of PHB scaffolds is 6000 rpm. The developed systems present a narrower diameter distribution and a higher fiber yield (Figure S4, *Supplementary Information*) ($\boldsymbol{\eta}_P$> 70%, $Q_1$-$Q_3$ for 5, 10 and 15 wt % of n-Hap are 1.27-2.40, 1.07-1.74, 1.02-1.78 μm, and the corresponding $\overline{D_f}$ are 1.96 ± 0.87, 1.44 ± 0.46, 1.44 ± 0.59 μm, respectively).



This article is protected by copyright. All rights reserved.

Author Manuscript

10974628, 2021, 14, Downloaded from https://onlinelibrary.wiley.com/doi/10.1002/app.50139 by The University Of Texas Rio Grande Valley, Wiley Online Library on [19/12/2022]. See the Terms and Conditions (https://onlinelibrary.wiley.com/terms-and-conditions) on Wiley Online Library for rules of use; OA articles are governed by the applicable Creative Commons License

Author Manuscript

Figure 2 shows the effect of n-Hap concentration on the morphology and fiber diameter distribution for the PHB systems. The micrographs show small protrusions exclusively at 10 and 15 wt % of n-Hap, which could be associated with the formation of agglomerates, in a similar way to what was observed by Ramier *et al.*[7] in electrospun fibers. On the other hand, at a concentration of 5 wt % of n-Hap, an increase in the $Q_1$-$Q_3$ interval diameter and its dispersion was observed, in comparison with the system obtained without n-Hap, reflecting an increase of 0.92-1.76 µm to 1.27-2.40 µm. On the contrary, at 10 and 15 wt % there was a decrease in fiber diameter, maintaining a similar range to that of the reference system.

Based on the apparent viscosity of the polymer solutions (Figure 2f), PHB solutions showed an increase in viscosity for samples containing 10 wt % of n-Hap, while at 15 wt % a slight decrease was observed possibly due to the presence of agglomerates which prevented particle-polymer interaction. When the viscosity increases, the resistance to elongate the polymeric solution increases as well; therefore resulting in fibers with a larger diameter for the same angular speed. [24,25] The results at 5 wt % of n-Hap described in the previous paragraph presented an increase in the $\overline{D_f}$. In the case of 10 and 15 wt % of n-Hap, the big agglomerates presence may have had an additional effect on fiber diameter. Due to the agglomerates the well dispersed concentration of n-Hap in the precursor solution is less than the initially established concentration. Consequently, the results of the fiber diameters will not necessarily reflect the expected influence with the increase in n-Hap concentration. The agglomerates were observed to act as thinning points resulting in fibers of smaller diameters.



This article is protected by copyright. All rights reserved.

10974628, 2021, 14, Downloaded from https://onlinelibrary.wiley.com/doi/10.1002/app.50139 by The University Of Texas Rio Grande Valley, Wiley Online Library on [19/12/2022]. See the Terms and Conditions (https://onlinelibrary.wiley.com/terms-and-conditions) on Wiley Online Library for rules of use; OA articles are governed by the applicable Creative Commons License

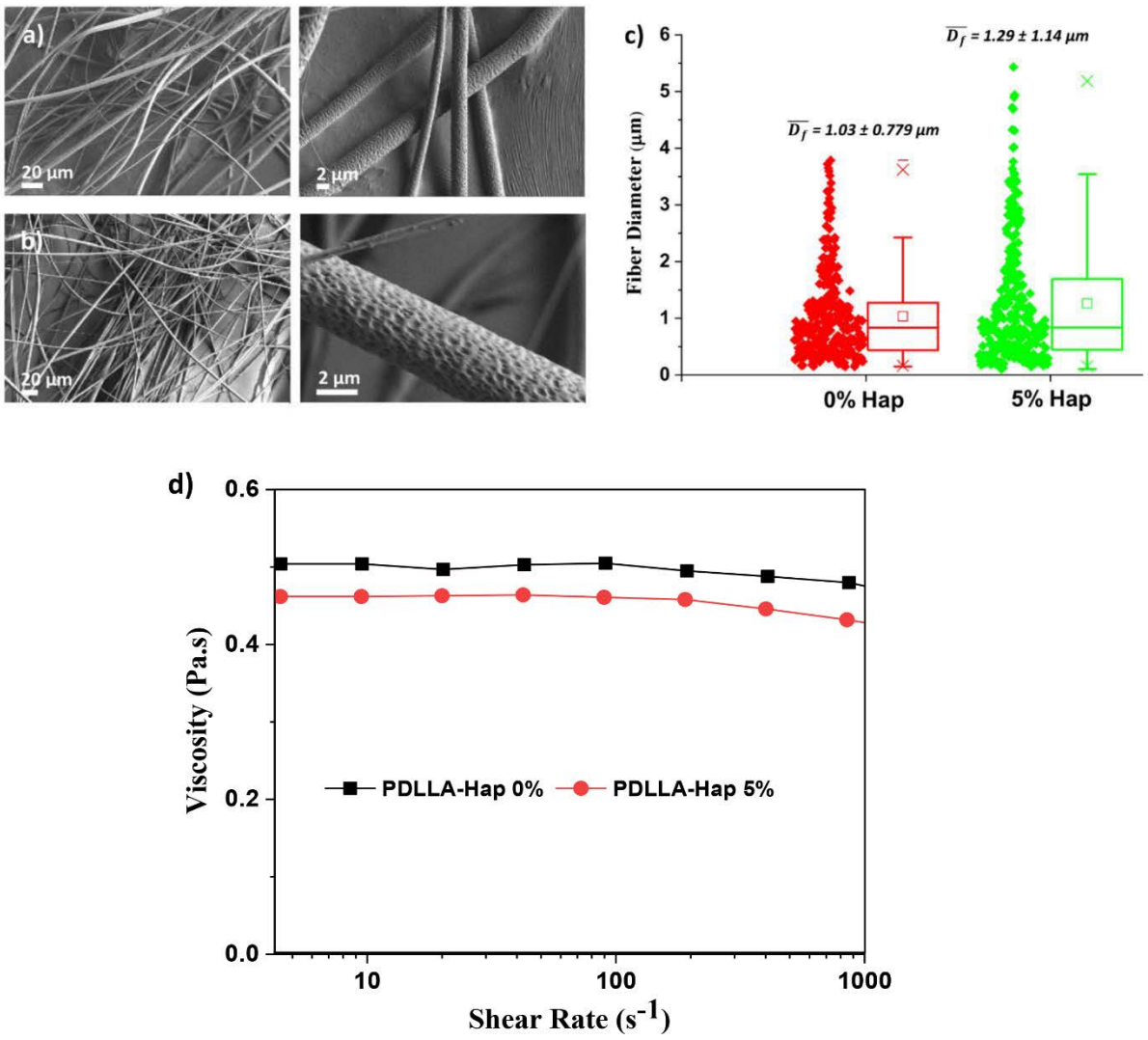


**Figure 1**.-SEM images of PDLLA systems at 0 wt % (a) and 5 wt % (b) of n-Hap obtained at ω of 7000 rpm, box charts of fiber diameters for each system (c) and rheological behavior of PDLLA solutions at 0 and 5 wt % of n-Hap (d).



This article is protected by copyright. All rights reserved.

Author Manuscript

10974628, 2021, 14, Downloaded from https://onlinelibrary.wiley.com/doi/10.1002/app.50139 by The University Of Texas Rio Grande Valley, Wiley Online Library on [19/12/2022]. See the Terms and Conditions (https://onlinelibrary.wiley.com/terms-and-conditions) on Wiley Online Library for rules of use; OA articles are governed by the applicable Creative Commons License

Author Manuscript



This article is protected by copyright. All rights reserved.

10974628, 2021, 14, Downloaded from https://onlinelibrary.wiley.com/doi/10.1002/app.50139 by The University Of Texas Rio Grande Valley, Wiley Online Library on [19/12/2022]. See the Terms and Conditions (https://onlinelibrary.wiley.com/terms-and-conditions) on Wiley Online Library for rules of use; OA articles are governed by the applicable Creative Commons License

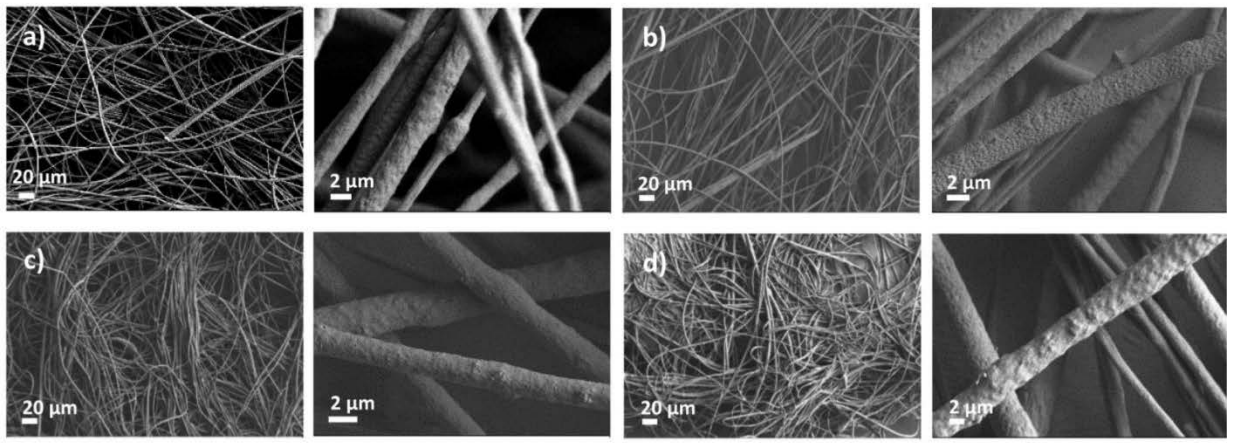


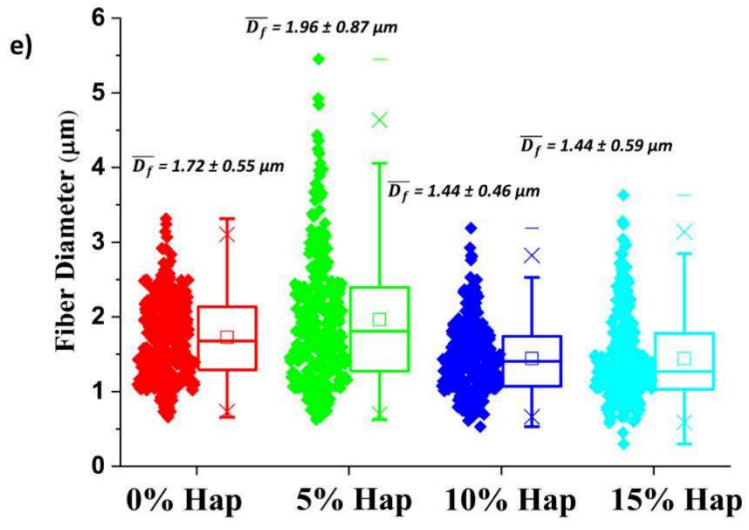


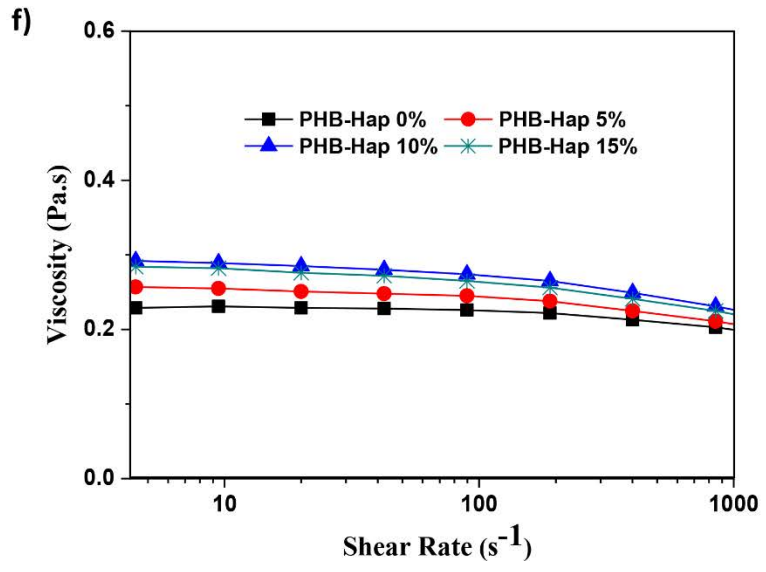




This article is protected by copyright. All rights reserved.

Author Manuscript

10974628, 2021, 14, Downloaded from https://onlinelibrary.wiley.com/doi/10.1002/app.50139 by The University Of Texas Rio Grande Valley, Wiley Online Library on [19/12/2022]. See the Terms and Conditions (https://onlinelibrary.wiley.com/terms-and-conditions) on Wiley Online Library for rules of use; OA articles are governed by the applicable Creative Commons License

**Figure 2**.- SEM images of PHB systems at 0 wt % (a), 5 wt % (b), 10 wt % (c) and 15 wt % (d) of n-Hap obtained at ω of 6000 rpm, box charts of fiber diameters for each system (e) and rheological behavior of PHB solutions at 0, 5, 10 and 15 wt % of n-Hap (d).

### *3.2.* Morphological characteristics of the designed hybrid materials

#### *3.2.1. Centrifugally spun PDLLA-Hap materials*

The images of the materials obtained under the conditions selected in the optimization stage are presented in Figure 3. The fibers mostly show a homogeneous appearance over their entire length (Figures 3a and b). The diameters dispersion was wider and shifted towards larger diameters (0.29-4.69 μm) when compared to the optimized system (0.10-3.58 μm). Regarding the n-Hap distribution, the presence of phosphorus was observed throughout the analyzed area (green dots in Figure 3d), indicative of a good distribution of the nanoparticles. The dispersion of the NPs was moderate, with some agglomerates along the fiber (Figure 3e). In addition, Figure 3g shows that n-Hap is mostly embedded within the fibers, probably due to its interaction with the polymer (see previous section), and as such preventing nanoparticles from transferring out of the matrix. A similar behavior was reported by Rizzi *et al.*[26], where under the same procedure of incorporating n-Hap into polymeric films based on polycaprolactone (PCL) and PLLA, NPs were observed to be embedded in the PLLA films, which evidences the presence of strong interactions between n-Hap and the polymer.

Additionally, fibers show a rough surface along the entire length. This roughness occurs mainly when a very volatile solvent (in this case, $CHCl_3$) is used for the preparation of the precursor solution, in combination with the fiber production in a relatively high atmospheric humidity (54.3% ± 8.7%).[27–29] Although the aforementioned variables are highly relevant to the surface appearance of the fibers, there are other factors such as solvent interaction with atmospheric water, water diffusion coefficient, and solubility parameters that also play key roles in surface morphology. [30]

The scaffold's porosity is above 90%, similar to fibers developed in our previously reported work.[31,32] Figure S5, *Supplementary Information*, shows the estimated scaffold pore sizes (spaces



This article is protected by copyright. All rights reserved.

Author Manuscript

10974628, 2021, 14, Downloaded from https://onlinelibrary.wiley.com/doi/10.1002/app.50139 by The University Of Texas Rio Grande Valley, Wiley Online Library on [19/12/2022]. See the Terms and Conditions (https://onlinelibrary.wiley.com/terms-and-conditions) on Wiley Online Library for rules of use; OA articles are governed by the applicable Creative Commons License

between fibers), specifically the 50% of the population which has an area above 30.52 μm$^2$ with most of the distribution in the 5 to 200 μm$^2$ range. These results pose promising potential for applications in tissue engineering.[33,34]

### *3.2.2. Centrifugally spun PHB-Hap materials*

Figure 4 shows the morphological characteristics of the PHB materials containing 5, 10 and 15 wt % of n-Hap, obtained at 6000 rpm. The fibers showed the expected behavior based on the previously performed morphological analysis; that is, mostly homogeneous fibers with a rough surface. The fiber diameter dispersion (Figures 4c, f, i) exhibited intervals similar to those observed in the optimization phase. However, in this case, the $Q_1$-$Q_3$ interval did not show significant variations between the systems, ranging from 1.2 to 2.3 μm.

Regarding the scaffolds' porosity, the values ranged from 93 to 96% (Figures 4c, f and i), while 50% of the pore population have an area above 31.8 ± 8 μm$^2$ and most of the population is distributed in a range from 2 to 200 μm$^2$ (Figure S6, *Supplementary Information*). In Figures 5a, d and g, the presence of phosphorus in the samples is shown. Through these images, a good distribution of the n-Hap is evidenced with agglomeration points that vary as n-Hap concentration increases. These results are consistent with those observed in the TEM images (Figures 5b, e and h), and the particles are mostly embedded within the fibers (Figures 5c, f and i).



This article is protected by copyright. All rights reserved.

Author Manuscript

10974628, 2021, 14, Downloaded from https://onlinelibrary.wiley.com/doi/10.1002/app.50139 by The University Of Texas Rio Grande Valley, Wiley Online Library on [19/12/2022]. See the Terms and Conditions (https://onlinelibrary.wiley.com/terms-and-conditions) on Wiley Online Library for rules of use; OA articles are governed by the applicable Creative Commons License

Author Manuscript

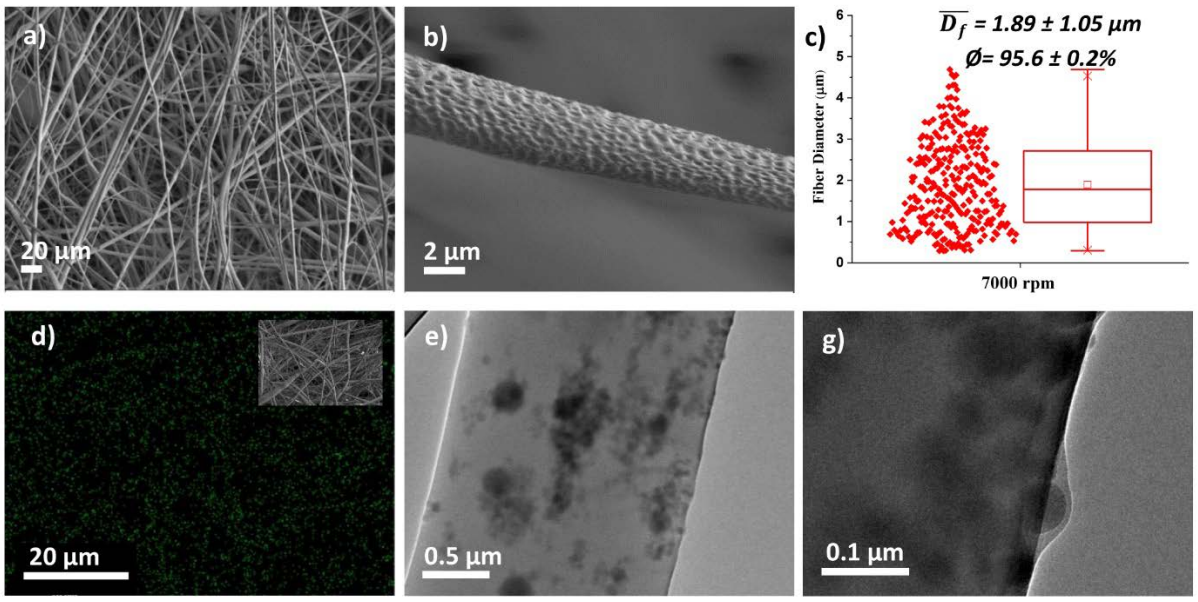


**Figure 3.** SEM images (a, b and d), TEM (f, g), box chart of fiber diameter (c) and mapping of element phosporous obtained through EDS of PDLLA-Hap 5% system produced at ω 7000 rpm.



This article is protected by copyright. All rights reserved.

10974628, 2021, 14, Downloaded from https://onlinelibrary.wiley.com/doi/10.1002/app.50139 by The University Of Texas Rio Grande Valley, Wiley Online Library on [19/12/2022]. See the Terms and Conditions (https://onlinelibrary.wiley.com/terms-and-conditions) on Wiley Online Library for rules of use; OA articles are governed by the applicable Creative Commons License

Author Manuscript

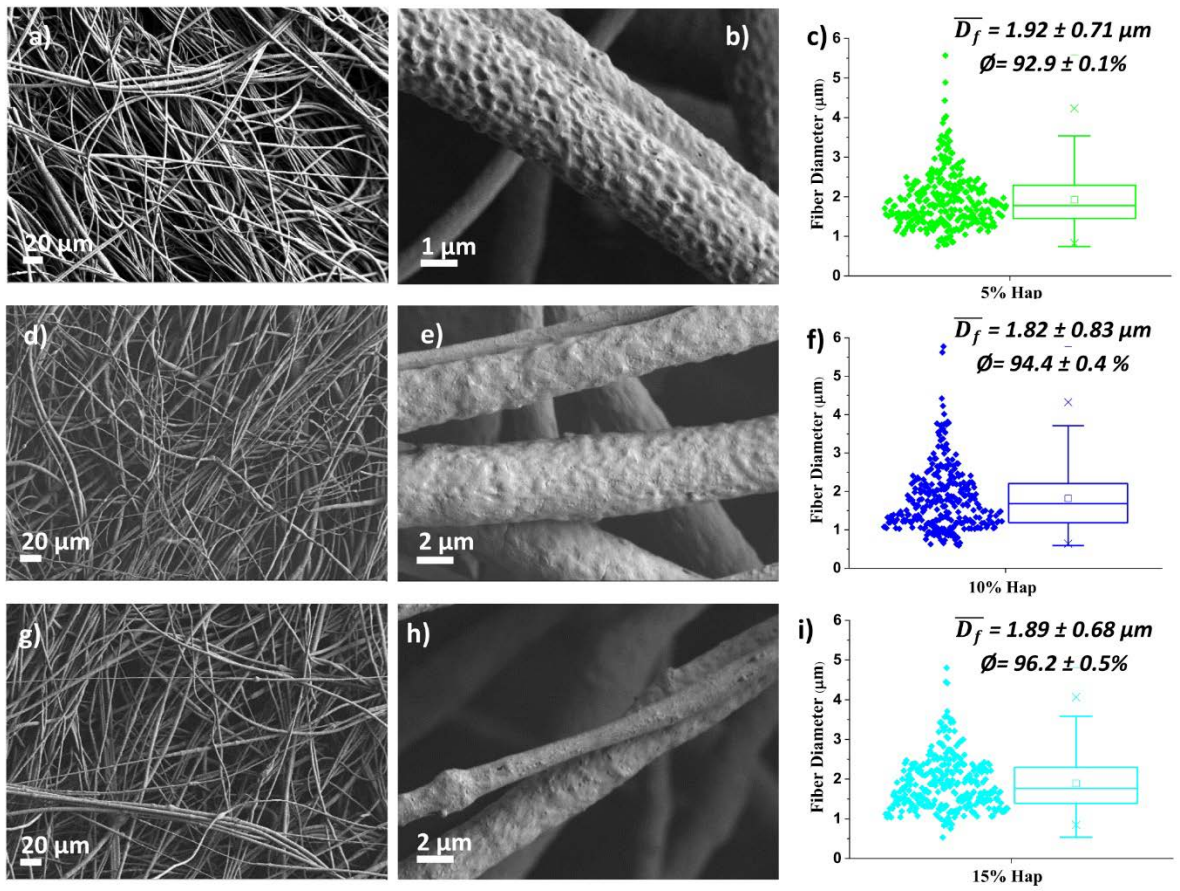


**Figure 4.-** SEM images (a, b, d, e, g, h) of PHB systems at 5 wt % (upper images), 10 wt % (middle images) and 15 wt % (lower images) of n-Hap, box charts of fiber diameters and their respective porosity (Ø) (c, f, i).



This article is protected by copyright. All rights reserved.

10974628, 2021, 14, Downloaded from https://onlinelibrary.wiley.com/doi/10.1002/app.50139 by The University Of Texas Rio Grande Valley, Wiley Online Library on [19/12/2022]. See the Terms and Conditions (https://onlinelibrary.wiley.com/terms-and-conditions) on Wiley Online Library for rules of use; OA articles are governed by the applicable Creative Commons License

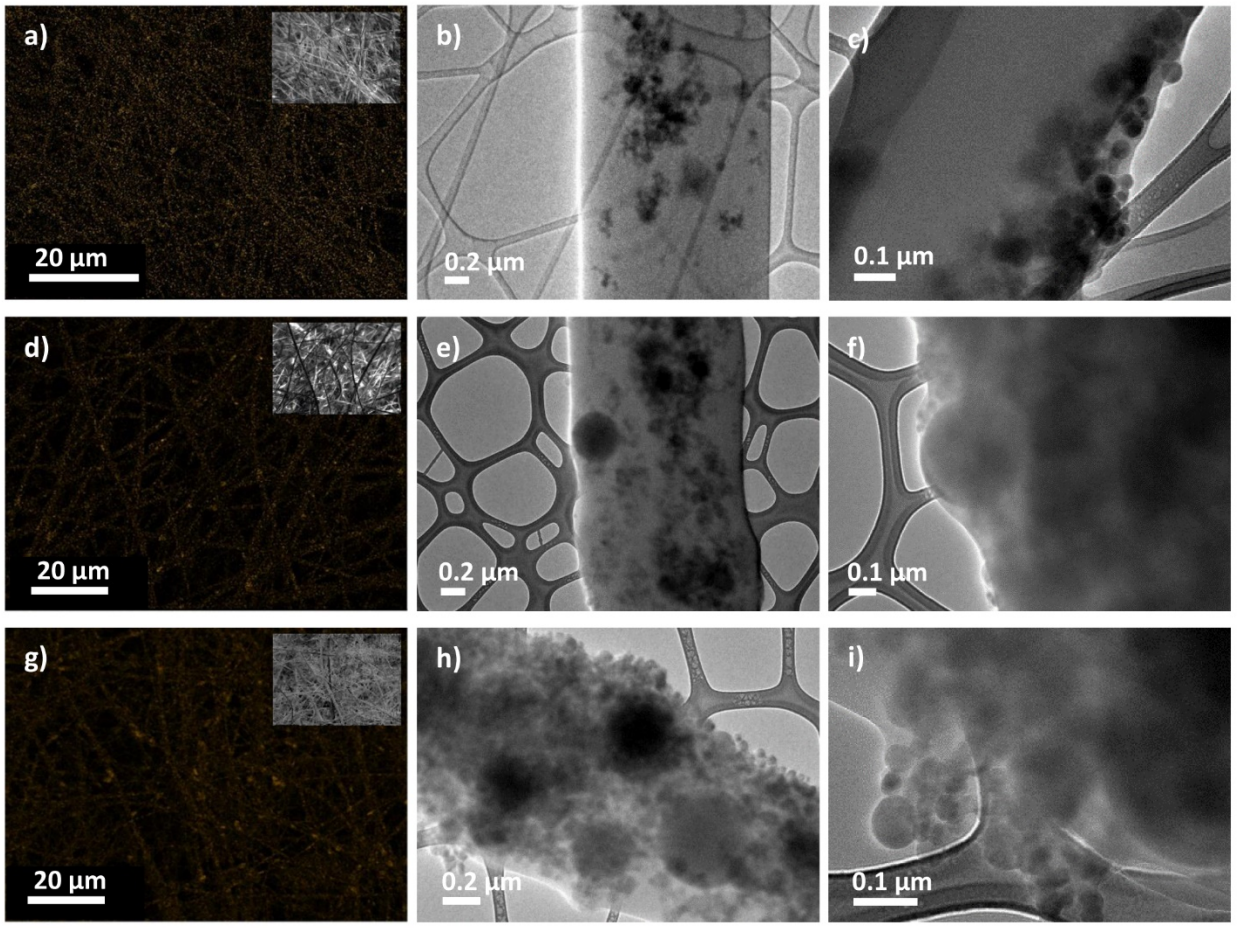


**Figure 5.-** Elemental mapping of phosphorous (a, b, g) and TEM images (d, c, e, f, h, i) of PHB systems at 5 wt % (upper images), 10 wt % (middle images) and 15 wt % (lower images) of n-Hap.

### 3.3. Thermal properties

From the thermo-degradation patterns of the scaffolds formulated with PDLLA (Figure 6a) and PHB (Figure 6b) at different n-Hap concentrations and at ω of 7000 and 6000 rpm, respectively, it was shown that the residues after heat treatment correspond to the theoretical concentration of n-Hap. Regarding the degradation of the materials, and taking into account the temperature at which the degradation rate reaches its maximum value ($T_d$) obtained by the derivative of the thermogram, it can be observed that the n-Hap did not produce a significant decrease in the thermal



This article is protected by copyright. All rights reserved.

Author Manuscript

10974628, 2021, 14, Downloaded from https://onlinelibrary.wiley.com/doi/10.1002/app.50139 by The University Of Texas Rio Grande Valley, Wiley Online Library on [19/12/2022]. See the Terms and Conditions (https://onlinelibrary.wiley.com/terms-and-conditions) on Wiley Online Library for rules of use; OA articles are governed by the applicable Creative Commons License

stability of the materials. In the case of PDLLA, a $T_d$ of 369 and 349 °C was obtained at 0 and 5% of n-Hap; respectively. On the other hand, the systems formulated with PHB showed a $T_d$ of 272, 262, 262 and 260 °C at 0, 5, 10 and 15wt % n-Hap, respectively. This behavior could be attributed to the hydroxyl groups of the Hap that act as a catalyst in the decomposition reaction of the polymer. [35]

Figure 7a shows the DSC thermograms of a heating-cooling-heating cycle of the PDLLA based scaffolds. In relation to the reference system (without n-Hap), in the first heating cycle an endothermic transition is observed at 62.5 °C with a relaxation enthalpy of 7,517 $J \cdot g^{-1}$, which occurs followed by the glass transition temperature ($T_g$) of the PDLLA (51.2 °C) (Figure S7, *Supplementary Information*). This behavior denotes the presence of a certain order of the polymer chains formed by the uniaxial stretching experienced by the polymeric fluid in the spinning process, a characteristic that had already been observed in previously published articles.[31,36,37] A similar behavior was observed at 5 wt % of n-Hap, but in this case the endothermic peak occurred at a higher temperature (63.3 °C) and enthalpy of relaxation (8.55 $J \cdot g^{-1}$), which evidences some NPs-polymeric matrix interaction. On the other hand, during cooling and second heating, there was only a second order transition ($T_g$) typical of an amorphous polymer, as expected.

In the case of PHB systems (Figure 7b) during the first heating cycle similar transitions are observed in systems with and without n-Hap, with negligible modifications to the melting temperatures. PHB is composed of 95% poly(3-hydroxybutyrate) (3-PHB), 4% poly(4-hydroxybutyrate) (4-PHB) and 1% polyhydroxyvalerate (3-PHV), therefore, in the first heating two endothermic peaks at 48 °C and 170 °C are identified, corresponding to the melting of the 4-PHB and 3-PHB crystalline phases, respectively.[32] Regarding the percentage of polymer crystallinity ($X_c$), the n-Hap caused a slight increase in $X_c$ at a concentration of 5 wt % and from 10 wt % (with a greater impact to 15wt %) a decrease was observed, being 47.4, 49.2, 43.0 and 40.0% for 0, 5, 10 and 15 wt % of n-Hap, respectively. In the cooling stage, a reduction in temperature and enthalpy of crystallization was evidenced by increasing the n-Hap concentration,



This article is protected by copyright. All rights reserved.

Author Manuscript

10974628, 2021, 14, Downloaded from https://onlinelibrary.wiley.com/doi/10.1002/app.50139 by The University Of Texas Rio Grande Valley, Wiley Online Library on [19/12/2022]. See the Terms and Conditions (https://onlinelibrary.wiley.com/terms-and-conditions) on Wiley Online Library for rules of use; OA articles are governed by the applicable Creative Commons License

similar to that described by Sánchez-Arévalo *et al.*[9] This behavior indicates that NPs are slowing the polymer crystallization process, possibly due to their interference during the packing of polymer chains.

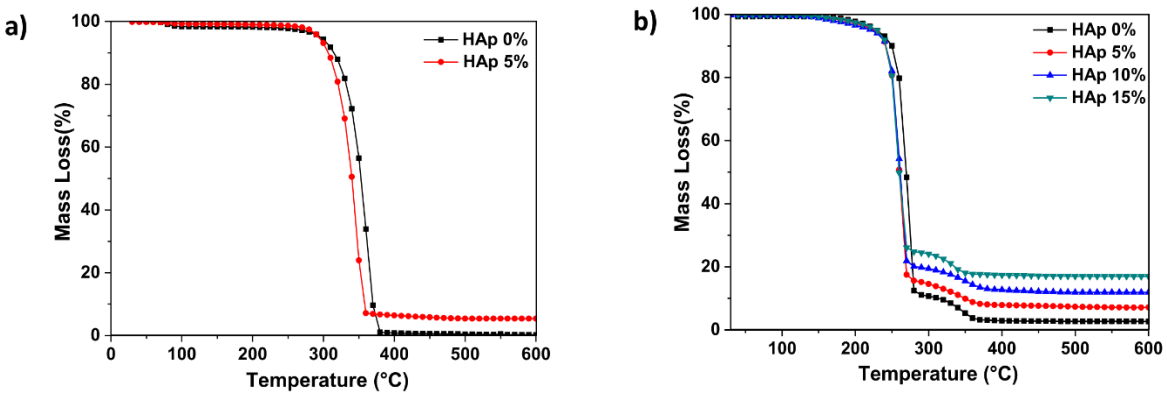


**Figure 6.** Degradation patterns derived from TGA of the centrifugally spun PDLLA (a) and PHB fibers (b) obtained at different concentrations of n-Hap.

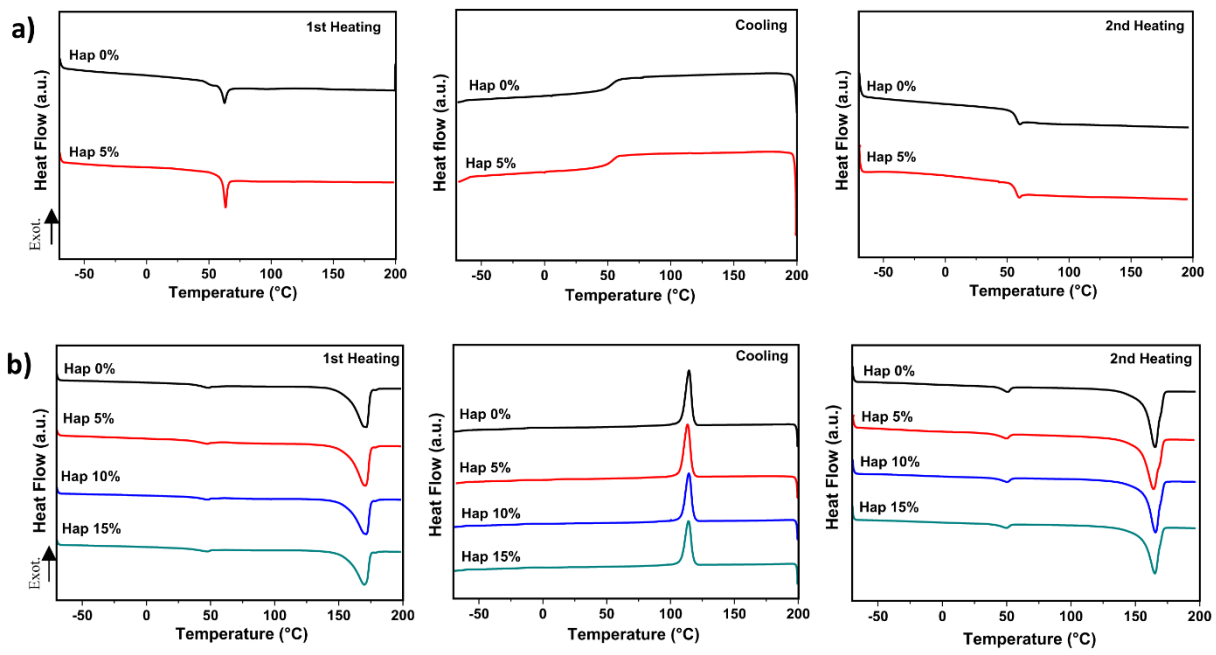




This article is protected by copyright. All rights reserved.

Author Manuscript

10974628, 2021, 14, Downloaded from https://onlinelibrary.wiley.com/doi/10.1002/app.50139 by The University Of Texas Rio Grande Valley, Wiley Online Library on [19/12/2022]. See the Terms and Conditions (https://onlinelibrary.wiley.com/terms-and-conditions) on Wiley Online Library for rules of use; OA articles are governed by the applicable Creative Commons License

**Figure 7.** DSC thermograms derived from one cycle of heating-cooling-heating of PDLLA a) and PHB b) fibrous mats at different concentration of n-Hap.

### 3.4. Mechanical properties

Figure 8 shows the stress-strain curves obtained from PDLLA and PHB control and hybrid systems; the Young´s modulus and the tensile strength are also shown. The fiber mats presented a linear elastic behavior in the first phase of deformation (elongation) and a maximum stress values before yielding at an elongation less than 10% and 20% for the PDLLA and PHB, respectively.

The selected fiber production method and chosen parameters significantly influence fiber orientation, polymer chain orientation, crystallinity, distribution of nanoparticles, as well as possible slipping between fibers, all of these factors then have an influence on the mechanical performance of the mats.[38,39] In the case of the PDLLA, a significant decrease in the Young's modulus and tensile strength with the incorporation of n-Hap was observed, specifically the percentage of reduction was 66.6 and 68.7 %, respectively. Other studies have reported similar results using different concentrations of n-Hap;[1,8,9] however, Gang Sui *et al.*,[40] reported an opposite result, adjudicating the behavior to the formation of strong surface bonding between the n-Hap and the polymer. In the case of PHB, the mechanical performance improved as the n-Hap concentration increased. Nevertheless, the decrease in the tensile strength presented at 15% could be due to the formation of n-Hap agglomerates that eventually acted as sites for crack propagation. In spite of this behavior, the tensile strength at 15% was higher than that one obtained without n-Hap. Ramier *et al.*[41] also observed an increase in the mechanical properties of hybrid fibrous mats obtained by the electrospinning technique.



This article is protected by copyright. All rights reserved.

Author Manuscript

10974628, 2021, 14, Downloaded from https://onlinelibrary.wiley.com/doi/10.1002/app.50139 by The University Of Texas Rio Grande Valley, Wiley Online Library on [19/12/2022]. See the Terms and Conditions (https://onlinelibrary.wiley.com/terms-and-conditions) on Wiley Online Library for rules of use; OA articles are governed by the applicable Creative Commons License

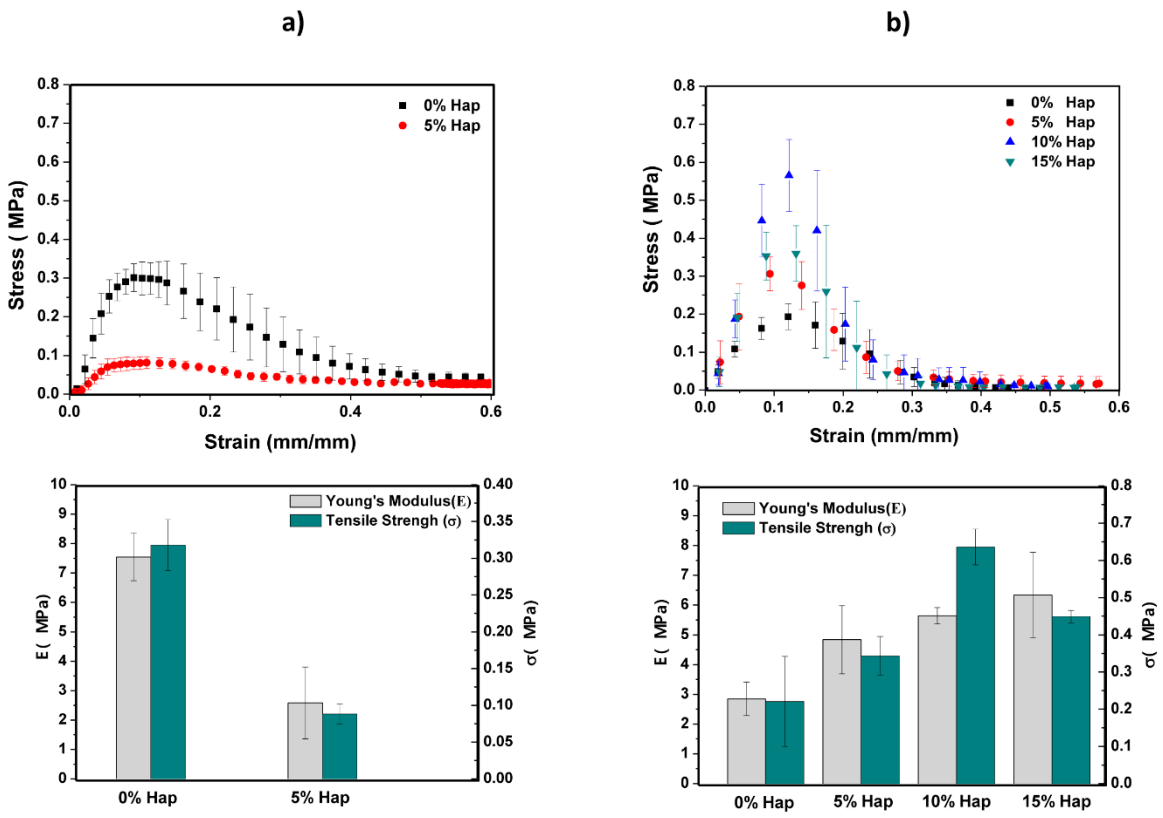


**Figure 8.** Stress-strain curves, Young's modulus (E) and tensile strength (σ) of the fiber mats obtained with PDLLA (a) and PHB (b) at different n-Hap concentrations.

### 3.5. Cell viability

Cell viability is a measure of the cell metabolic activity. The test was carried out through the fluorescence emitted by a redox indicator, known as resazurin, which is effectively reduced in cells mitochondria producing resorufin. This final product is excreted to the culture medium, making it a source to evaluate the cell mitochondrial metabolic activity.

It is important to highlight that for this test, only the systems obtained at 5% n-Hap and their corresponding references were evaluated for comparative purposes. In Figure 9, the influence of the designed materials on the behavior of Saos-2 (Osteoblast-like) cells can be observed. Regarding the polymer type, it is clear that PDLLA produced a better cellular response than PHB,



This article is protected by copyright. All rights reserved.

Author Manuscript

10974628, 2021, 14, Downloaded from https://onlinelibrary.wiley.com/doi/10.1002/app.50139 by The University Of Texas Rio Grande Valley, Wiley Online Library on [19/12/2022]. See the Terms and Conditions (https://onlinelibrary.wiley.com/terms-and-conditions) on Wiley Online Library for rules of use; OA articles are governed by the applicable Creative Commons License

with a cell viability of around 60%. On the other hand, PDLLA-Hap 5% system promoted an increase of 10% in cell viability by day 7. The observed behavior could be attributed to the NPs disposition on the material, as they are mostly embedded in the fibers, avoiding the NPs direct interaction with the cells at first and third day of experimentation. With regard to the seventh day, it is likely that surface erosion (hydrolytic degradation)[27] of the fibers produced the exposure of a greater number of NPs, causing an increase in the cell metabolic activity. In addition, different authors have reported that n-Hap promote the superficial mineralization of apatite;[42,43] which could have had an effect on the final result. In the case of PHB-Hap 5%, no significant changes in cell viability were observed when compared to the PHB without n-Hap. The decreased viability with days of interaction could indicate the presence of a certain cytotoxic effect in the cells. Different works have reported similar results regarding the lack of n-Hap effect on the viability and proliferation of osteoblast cells, while its influence on other mechanisms that allow its osteogenic evaluation in different cell lines, have shown a notable positive effect.[6,8,40,41,44]

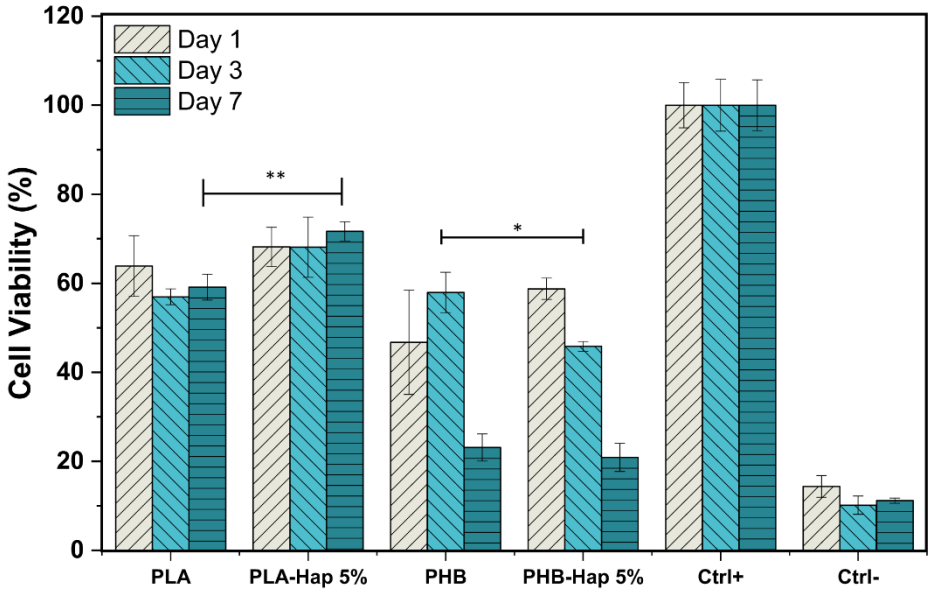




This article is protected by copyright. All rights reserved.

Author Manuscript

10974628, 2021, 14, Downloaded from https://onlinelibrary.wiley.com/doi/10.1002/app.50139 by The University Of Texas Rio Grande Valley, Wiley Online Library on [19/12/2022]. See the Terms and Conditions (https://onlinelibrary.wiley.com/terms-and-conditions) on Wiley Online Library for rules of use; OA articles are governed by the applicable Creative Commons License

**Figure 9.** Osteoblast cell viability evaluated through days 1, 3, and 7 with resazurin. A statistical analysis is shown measuring the standard deviation of the mean, n= 3 trial experiment (* $p < 0.05$, ** $p < 0.01$).

## 4. Conclusions

PHB showed greater versatility for the production of homogeneous fibers at different n-Hap concentrations (5, 10 and 15 wt %) compared to PDLLA (5 wt %). The hybrid systems obtained presented rough surfaces, and thermal stability similar to those of fibrous materials without n-Hap. In addition, n-Hap acted as a reinforcement for PHB systems, in which a better mechanical performance was observed at a concentration of 10 wt %; the contrary occurred in the PDLLA based systems. Regarding cell viability, PDLLA systems promoted higher cellular response than those formulated with PHB. Moreover, for PDLLA systems, the incorporation of n-Hap produced a significant difference in the metabolic activity of Saos-2 cells by day seven of the assay. On the other hand, no significant changes were observed in PHB systems.

## 5. Acknowledgments

The authors thank CONACyT for the scholarship granted (429352) to Victoria Padilla Gainza, and for the support received by the National Science Foundation (NSF DMR 1523577). The authors also thank Anabel Ochoa, Alejandro Castillo, and Jesús G. Quiroz López for their technical assistance related to the evaluation of thermal properties, images by SEM and mechanical properties, respectively.

## 6. References

1. Morelli, S., Salerno, S., Holopainen, J., Ritala, M., De Bartolo, L. Osteogenic and osteoclastogenic differentiation of co-cultured cells in polylactic acid-nanohydroxyapatite fiber scaffolds. *J Biotechnol*. **2015**;204:53-62.
2. Ripamonti, U. Osteoinduction in porous hydroxyapatite implanted in heterotopic site of different animal models. *Biomaterials*. **1996**;17(1):31-35.



This article is protected by copyright. All rights reserved.

Author Manuscript

10974628, 2021, 14, Downloaded from https://onlinelibrary.wiley.com/doi/10.1002/app.50139 by The University Of Texas Rio Grande Valley, Wiley Online Library on [19/12/2022]. See the Terms and Conditions (https://onlinelibrary.wiley.com/terms-and-conditions) on Wiley Online Library for rules of use; OA articles are governed by the applicable Creative Commons License

Author Manuscript


3. Albrektsson, T., Johansson, C. Osteoinduction, osteoconduction and osseointegration. *Eur Spine J*. **2001**;10:S96-S101.

4. Zhou, H., Lawrence, J.G., Bhaduri, S.B. Fabrication aspects of PLA-CaP/PLGA-CaP composites for orthopedic applications: A review. *Acta Biomater*. **2012**;8(6):1999-2016.

5. Koo, A., Ohe, J-Y., Lee, D-W., Chun, J., Lee, H-J., Kown, Y-D. and Lee S-C. Bone-regenerative activity of parathyroid hormone-releasing nano-hydroxyapatite/poly(L-lactic acid) hybrid scaffolds. *Macromol Res*. **2015**;23(12):1168-1173.

6. Sadat-Shojai, M., Khorasani, MT., Jamshidi, A. A new strategy for fabrication of bone scaffolds using electrospun nano-HAp/PHB fibers and protein hydrogels. *Chem Eng J*. **2016**;289:38-47.

7. Ramier, J., Bouderlique, T., Stoilova, O., Manolova, N., Rashkov, I., Langlois, V., Renard, E., Albanese, P. and Grande, D. Biocomposite scaffolds based on electrospun poly ( 3-hydroxybutyrate ) nano fibers and electrosprayed hydroxyapatite nanoparticles for bone tissue engineering applications. *Mater Sci Eng C*. **2014**;38:161-169.

8. Novotna, K., Zajdlova, M., Suchy, T., Hadraba, D., Lopot, F., Zaloudkova, M., Douglas, T., Munzarova, M., Juklickova, M., Stranska, D., Kubies, D., Schaubroeck, D., Wille, S., Balcaen, L., Jarosova, M., Kozak, Ha., Kromka, A., Svindrych, Z., Lisa, V., Balik, K. and Bacakova, L. Polylactide nanofibers with hydroxyapatite as growth substrates for osteoblast-like cells. *J Biomed Mater Res - Part A*. **2014**;102(11):3918-3930.

9. Sánchez-Arévalo, F. M., Muñoz-Ramírez, L. D., Álvarez-Camacho, M., Rivera-Torres, F., Maciel-Cerda, A., Montiel-Campos, R. and Vera-Graziano, R. Macro- and micromechanical behaviors of poly(lactic acid)–hydroxyapatite electrospun composite scaffolds. *J Mater Sci*. **2017**;52(6):3353-3367.

10. Zhang X, Lu Y. Centrifugal Spinning: An Alternative Approach to Fabricate Nanofibers at High Speed and Low Cost. *Polym Rev*. **2014**;54(4):677-701.

11. Thoppey, N.M., Bochinski, J.R., Clarke, L.I., Gorga, R.E. Edge electrospinning for high throughput production of quality nanofibers. *Nanotechnology*. **2011**;22(34).

12. Padron, S., Fuentes, A., Caruntu, D., Lozano, K. Experimental study of nanofiber production through forcespinning. *J Appl Phys*. **2013**;113:24318.

13. Sebe, I., Szabó, B., Nagy, Z. K., Szabó, D., Zsidai, L., Kocsis, B. and Zelkó, R. Polymer structure and antimicrobial activity of polyvinylpyrrolidone-based iodine nanofibers prepared with high-speed rotary spinning technique. *Int J Pharm*. **2013**;458(1):99-103.

14. Padron, S.; Patlan, R.; Gutierrez, J.; Santos, N.; Eubanks, T.; Lozano K. Production and characterization of hybrid BEH-PPV/PEO conjugated polymer nanofibers by ForcespinningTM. *J Appl Polym Sci*. **2012**;125:3610-3616.

15. Wang, Z., Zhao, C., Pan, Z. Porous bead-on-string poly(lactic acid) fibrous membranes for




This article is protected by copyright. All rights reserved.

10974628, 2021, 14, Downloaded from https://onlinelibrary.wiley.com/doi/10.1002/app.50139 by The University Of Texas Rio Grande Valley, Wiley Online Library on [19/12/2022]. See the Terms and Conditions (https://onlinelibrary.wiley.com/terms-and-conditions) on Wiley Online Library for rules of use; OA articles are governed by the applicable Creative Commons License

Author Manuscript

air filtration. *J Colloid Interface Sci*. **2015**;441:121-129.

16. Lopresti, F., Carfi Pavia, F., Vitrano, I., Kersaudy-Kerhoas, M., Brucato, V., La Carrubba, V. Effect of hydroxyapatite concentration and size on morpho-mechanical properties of PLA-based randomly oriented and aligned electrospun nanofibrous mats. *J Mech Behav Biomed Mater*. **2020**;101, 103449.
17. Jacquel, N., Lo, C-W., Wu, H-S., Wei, Y-H., Wang, SS. Solubility of Polyhydroxyalkanoates by Experiment and Thermodynamic Correlations. *AIChE J*. **2007**;53(10):2704-2714.
18. Rogalski, J.J., Bastiaansen, CWM., Peijs, T. Rotary jet spinning review–a potential high yield future for polymer nanofibers. *Nanocomposites*. **2017**;3(4):97-121.
19. Wong, S.C., Baji, A., Leng, S. Effect of fiber diameter on tensile properties of electrospun poly(ε-caprolactone). *Polymer*. **2008**;49(21):4713-4722.
20. Neuendorf, RE., Saiz, E., Tomsia, A. P., Ritchie, R.O. Adhesion between biodegradable polymers and hydroxyapatite: Relevance to synthetic bone-like materials and tissue engineering scaffolds. *Acta Biomater*. **2008**;4(5):1288-1296.
21. Shaobing, Z., Xiaotong, Z., Xiongjun, Y., Jianxin, W., Jie, W., Xiaohong, L., Bo, F., Ming, Y. Hydrogen Bonding Interaction of Poly( d , l -Lactide)/hydroxyapatite Nanocomposites. *Chem Mater*. **2007**;19(2):247-253.
22. Othman, N. Rheology and Processing of Poly ( Lactides ) and Their Enantiomeric Copolymers and Blends .(The University of British Columbia, **2012**).
23. Chae, D.W., Kim, B.C. Effects of interface affinity on the rheological properties of zinc oxide nanoparticle-suspended polymer solutions. *Macromol Res*. **2010**;18(8):772-776.
24. Hong, X., Edirisinghe, M., Mahalingam, S. Beads, beaded-fibres and fibres: Tailoring the morphology of poly(caprolactone) using pressurised gyration. *Mater Sci Eng C*. **2016**;69:1373-1382.
25. Adam, M., Delsanti, M. Viscosity of semi-dilute polymer solutions. *J Phys*. **1982**;43(3):549-557.
26. Rizzi, S.C. Biodegratdable polymer/hydroxyapatite composites: Surface analysis and initial attachment of human osteoblasts. *J Biomed Mater Res*. **2001**;55:475-486.
27. Casper, C.L., Stephens, J.S., Tassi, N.G., Chase, D.B., Rabolt, J.F. Controlling surface morphology of electrospun polystyrene fibers: Effect of humidity and molecular weight in the electrospinning process. *Macromolecules*. **2004**;37(2):573-578.
28. Shenoy, S.L., Bates, W.D., Frisch, H.L., Wnek, G.E. Role of chain entanglements on fiber formation during electrospinning of polymer solutions: Good solvent, non-specific polymer-polymer interaction limit. *Polymer*. **2005**;46(10):3372-3384.



This article is protected by copyright. All rights reserved.

10974628, 2021, 14, Downloaded from https://onlinelibrary.wiley.com/doi/10.1002/app.50139 by The University Of Texas Rio Grande Valley, Wiley Online Library on [19/12/2022]. See the Terms and Conditions (https://onlinelibrary.wiley.com/terms-and-conditions) on Wiley Online Library for rules of use; OA articles are governed by the applicable Creative Commons License

Author Manuscript


29. Megelski, S., Stephens, J.S., Bruce Chase, D., Rabolt, J.F. Micro- and nanostructured surface morphology on electrospun polymer fibers. *Macromolecules*. **2002**;35(22):8456-8466.

30. Lakshmi, N., Jackie, N., Aravind, D., Suzhu, Y., Manan, M.A. Surface Morphology of Electrospun PLA fibers: Mechanisms of pore formation. *RSC Adv*. **2014**;4(83):44082-44088.

31. Padilla-Gainza, V., Morales, G., Rodríguez-Tobías, H., Lozano, K. Forcespinning technique for the production of poly(d,l-lactic acid) submicrometer fibers: Process–morphology–properties relationship. *J Appl Polym Sci*. **2019**;136(22):1-9.

32. Padilla-Gainza, V., Rodríguez-Tobías, H., Morales, G., Ledezma-Pérez, A., Alvarado-Canché, Ca., Rodríguez, C., Gilkerson, R., Lozano, K. Processing-structure-property relationships of biopolyester/zinc oxide fibrous scaffolds engineered by centrifugal spinning. *Polym Adv Technol*. **2020**:1-14.

33. Porter, J.R., Ruckh, T.T., Popat, K.C. Bone tissue engineering: A review in bone biomimetics and drug delivery strategies. *Biotechnol Prog*. **2009**;25(6):1539-1560.

34. Kumbar, S.G., James, R., Nukavarapu, S.P, Laurencin, C.T. Electrospun nanofiber scaffolds: engineering soft tissues. *Biomed Mater*. **2008**;3:1-15.

35. Bikiaris, D.N. Nanocomposites of aliphatic polyesters: An overview of the effect of different nanofillers on enzymatic hydrolysis and biodegradation of polyesters. *Polym Degrad Stab*. **2013**;98(9):1908-1928.

36. Anžlovar, A., Kržan, A., Žagar, E. Degradation of PLA/ZnO and PHBV/ZnO composites prepared by melt processing. *Arab J Chem*. **2018**, 11, 343-352.

37. Ishii, Y., Omori, K., Sakai, H., Arakawa, Y., Fukuda, M. Versatile Approach for Reducing Propagation Loss in Wet-Electrospun Polymer Fiber Waveguides. *ACS Omega*. **2018**;3(6):6787-6793.

38. Andrady, A.L. Characterization of Nanofibers and Mats. In: *Science and Technology of Polymer Nanofibers*. Hoboken: John Wiley&Sons; **2007**:133-138. chapter 5, pp 111-152.

39. Singh, J.P., Verma, S. Raw materials for terry fabrics. In: *Woven Terry Fabrics*. Amsterdam: Woodhead Publishing; **2016**: chapter 3, pp 19-28.

40. Sui, G., Yang, X., Mei, F., Hu, X., Chen, G., Deng, X., Ryu, S. Poly-L-lactic acid/hydroxyapatite hybrid membrane for bone tissue regeneration. *Wiley Intersci*. **2007**;33:446-454.

41. Ramier, J., Bouderlique, T., Stoilova, O., Manolova, N., Rashkov, I., Langlois, V., Renard, E., Albanese, P., Grande, D. Biocomposite scaffolds based on electrospun poly ( 3-hydroxybutyrate ) nano fi bers and electrosprayed hydroxyapatite nanoparticles for bone tissue engineering applications. *Mater Sci Eng C*. **2014**;38:161-169.




This article is protected by copyright. All rights reserved.

10974628, 2021, 14, Downloaded from https://onlinelibrary.wiley.com/doi/10.1002/app.50139 by The University Of Texas Rio Grande Valley, Wiley Online Library on [19/12/2022]. See the Terms and Conditions (https://onlinelibrary.wiley.com/terms-and-conditions) on Wiley Online Library for rules of use; OA articles are governed by the applicable Creative Commons License

42. Palmer, L.C., Newcomb, C.J., Kaltz, S.R., Spoerke, E.D., Stupp, S.I. Biomimetic systems for hydroxyapatite mineralization inspired by bone and enamel. *Chem Rev*. **2008**;108(11):4754-4783.

43. Lao, L., Zhu, Y., Zhang, Y., Gao, Z., Zhou, F., Chen, L., Ouyang, H., Gao, C. Mineralization of collagen-coated electrospun poly(lactide-co-glycolide) nanofibrous mesh to enhance growth and differentiation of osteoblasts and bone marrow mesenchymal stem cells. *Adv Eng Mater*. **2012**;14(4):123-137.

44. Rivero, G., Furtos, G., Abraham, G. Amoxicillin-Loaded Electrospun Scaffolds Based on Polycaprolactone and Nanohydroxyapatite for Dental Applications. In: *XI Simposio Argentino de Polímeros - SAP 2015*. Santa Fé; Oct 20-23, **2015**, 571-575.



This article is protected by copyright. All rights reserved.

Author Manuscript

10974628, 2021, 14, Downloaded from https://onlinelibrary.wiley.com/doi/10.1002/app.50139 by The University Of Texas Rio Grande Valley, Wiley Online Library on [19/12/2022]. See the Terms and Conditions (https://onlinelibrary.wiley.com/terms-and-conditions) on Wiley Online Library for rules of use; OA articles are governed by the applicable Creative Commons License

Author Manuscript

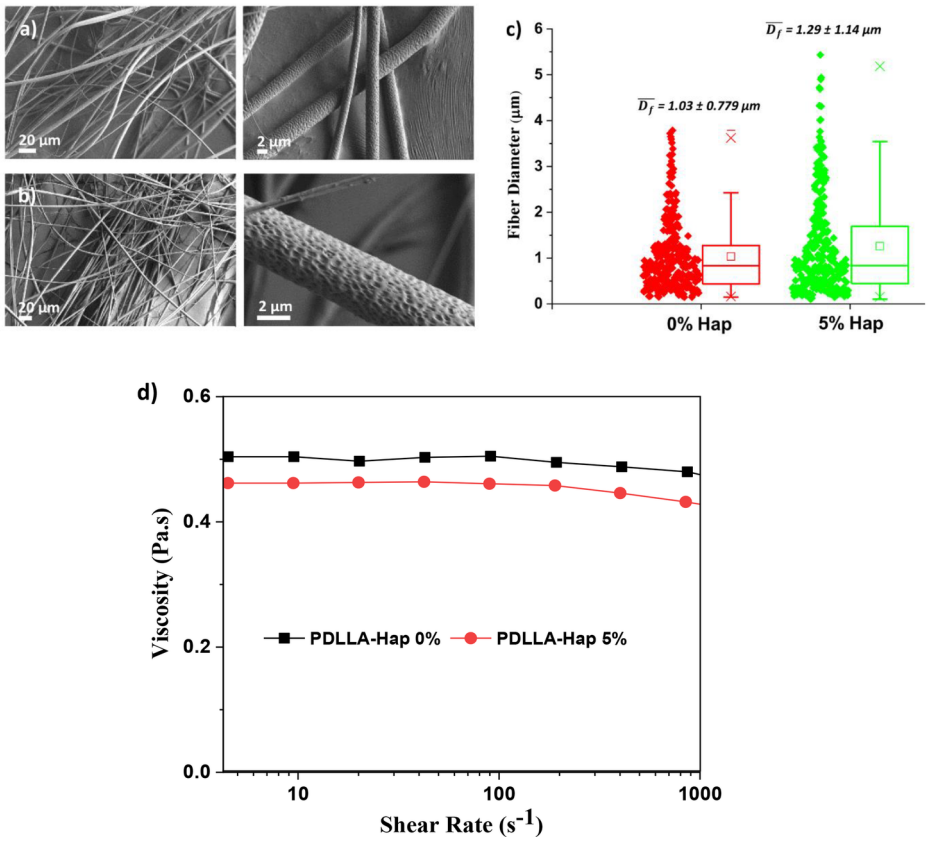


APP_50139_Figure 1.tif

This article is protected by copyright. All rights reserved.

10974628, 2021, 14, Downloaded from https://onlinelibrary.wiley.com/doi/10.1002/app.50139 by The University Of Texas Rio Grande Valley, Wiley Online Library on [19/12/2022]. See the Terms and Conditions (https://onlinelibrary.wiley.com/terms-and-conditions) on Wiley Online Library for rules of use; OA articles are governed by the applicable Creative Commons License

Author Manuscript

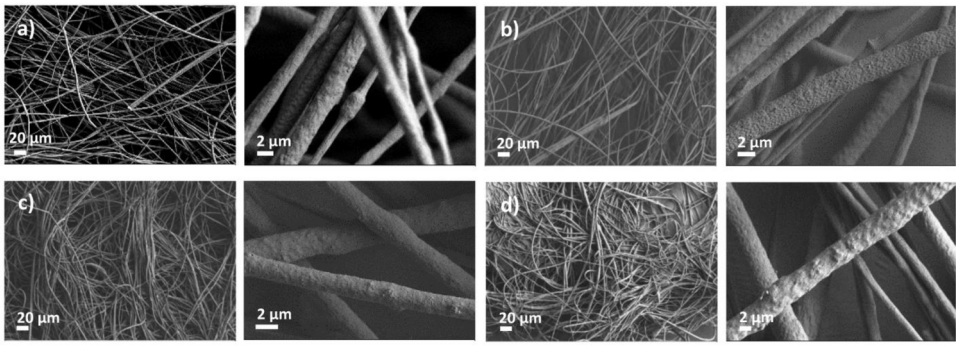


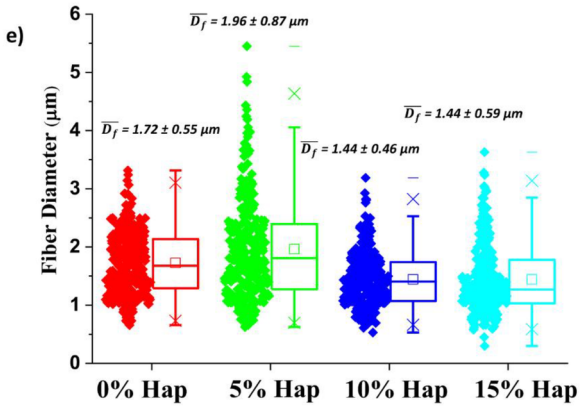


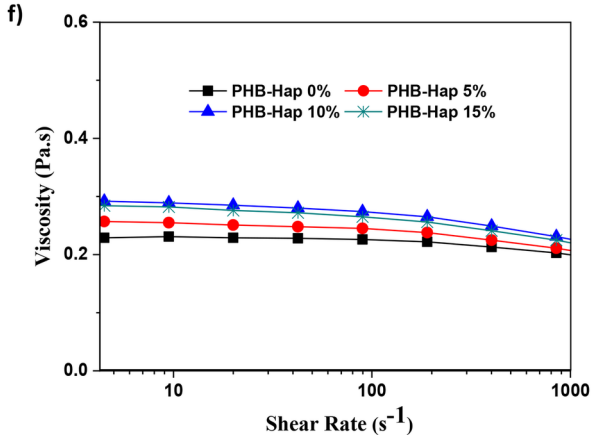


APP_50139_Figure 2.tif

This article is protected by copyright. All rights reserved.

10974628, 2021, 14, Downloaded from https://onlinelibrary.wiley.com/doi/10.1002/app.50139 by The University Of Texas Rio Grande Valley, Wiley Online Library on [19/12/2022]. See the Terms and Conditions (https://onlinelibrary.wiley.com/terms-and-conditions) on Wiley Online Library for rules of use; OA articles are governed by the applicable Creative Commons License

Author Manuscript

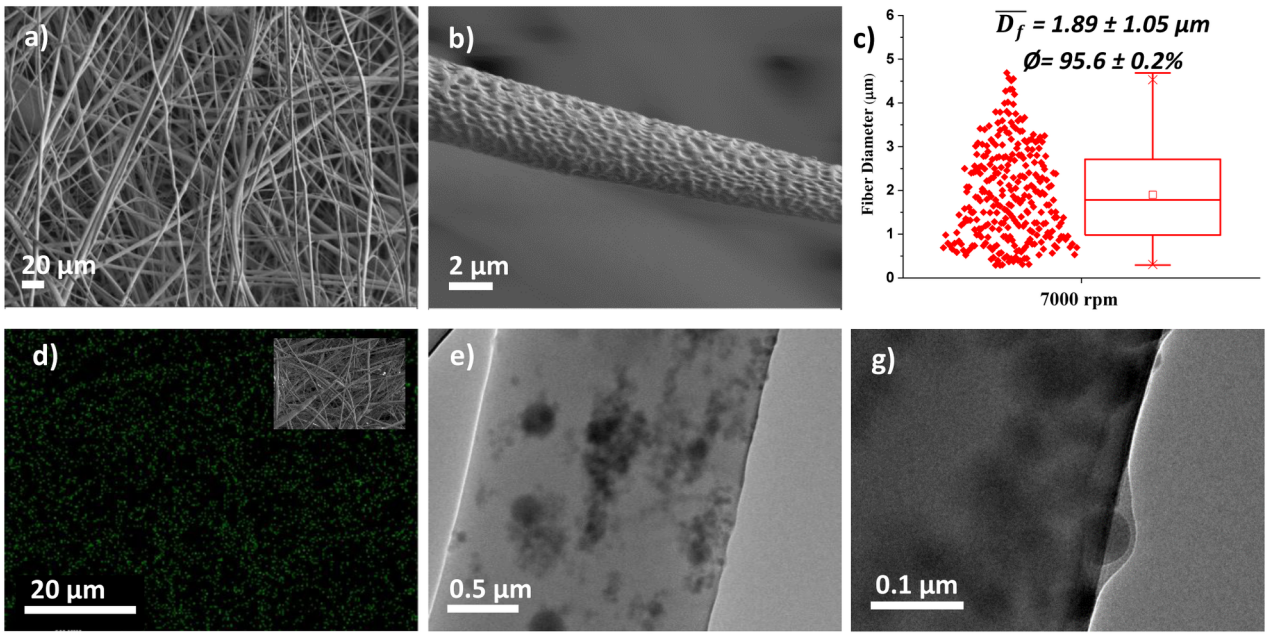


APP_50139_Figure 3.tif

This article is protected by copyright. All rights reserved.

10974628, 2021, 14, Downloaded from https://onlinelibrary.wiley.com/doi/10.1002/app.50139 by The University Of Texas Rio Grande Valley, Wiley Online Library on [19/12/2022]. See the Terms and Conditions (https://onlinelibrary.wiley.com/terms-and-conditions) on Wiley Online Library for rules of use; OA articles are governed by the applicable Creative Commons License

Author Manuscript

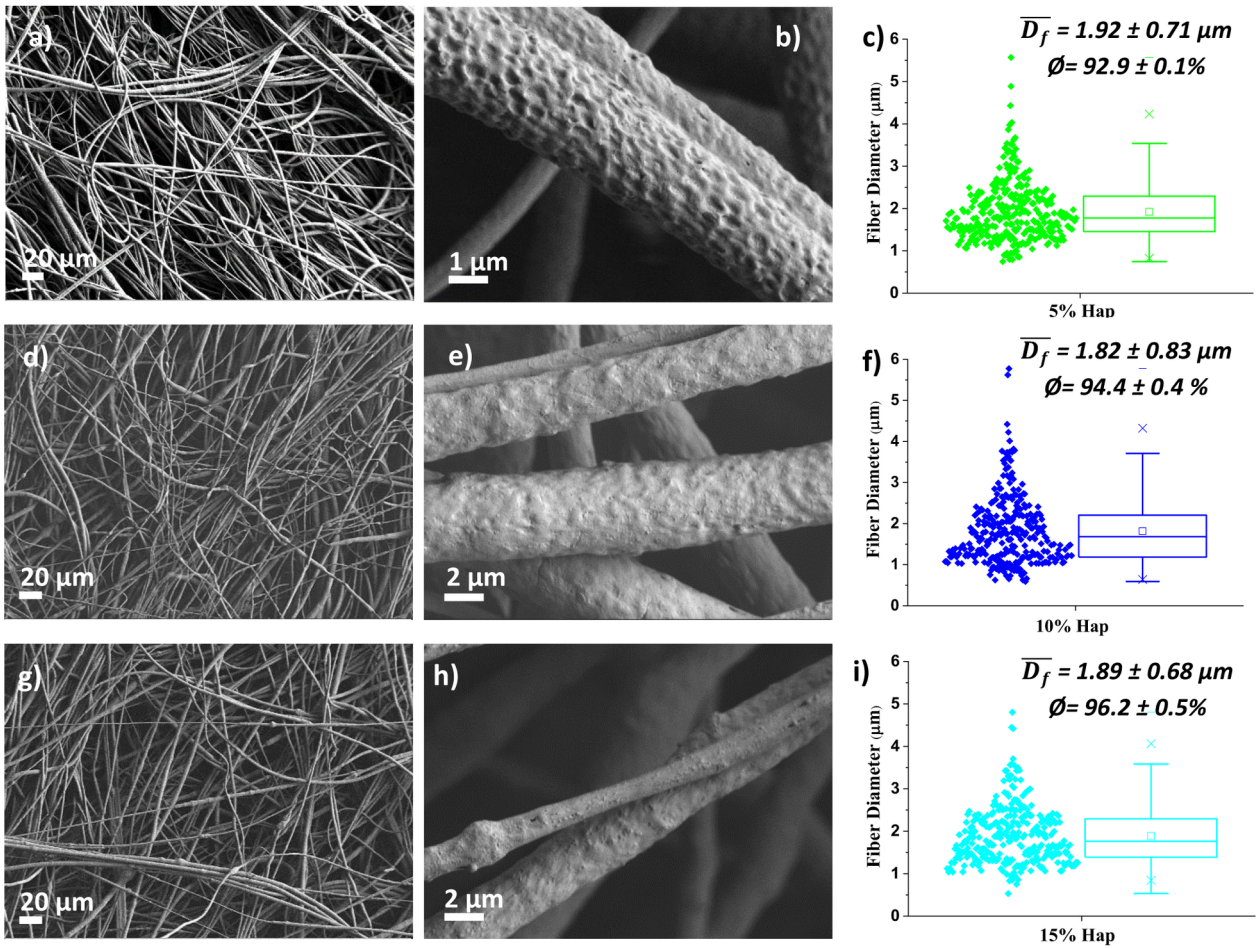


APP_50139_Figure 4.tif

This article is protected by copyright. All rights reserved.

10974628, 2021, 14, Downloaded from https://onlinelibrary.wiley.com/doi/10.1002/app.50139 by The University Of Texas Rio Grande Valley, Wiley Online Library on [19/12/2022]. See the Terms and Conditions (https://onlinelibrary.wiley.com/terms-and-conditions) on Wiley Online Library for rules of use; OA articles are governed by the applicable Creative Commons License

Author Manuscript

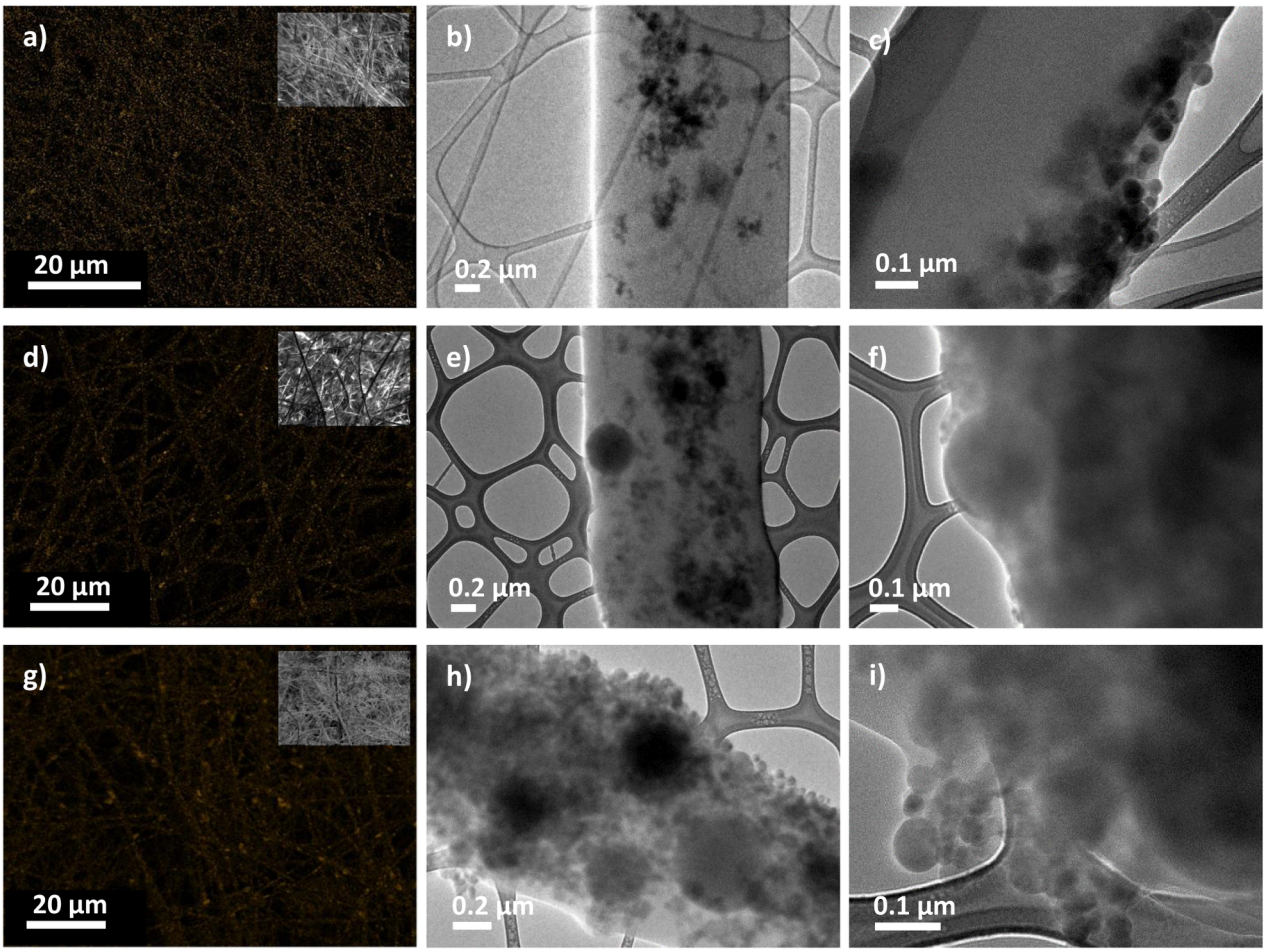


APP_50139_Figure 5.tif

This article is protected by copyright. All rights reserved.

10974628, 2021, 14, Downloaded from https://onlinelibrary.wiley.com/doi/10.1002/app.50139 by The University Of Texas Rio Grande Valley, Wiley Online Library on [19/12/2022]. See the Terms and Conditions (https://onlinelibrary.wiley.com/terms-and-conditions) on Wiley Online Library for rules of use; OA articles are governed by the applicable Creative Commons License

Author Manuscript

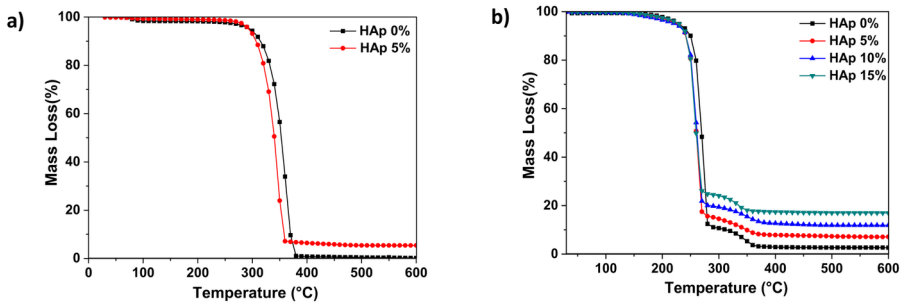


APP_50139_Figure 6.tif

This article is protected by copyright. All rights reserved.

10974628, 2021, 14, Downloaded from https://onlinelibrary.wiley.com/doi/10.1002/app.50139 by The University Of Texas Rio Grande Valley, Wiley Online Library on [19/12/2022]. See the Terms and Conditions (https://onlinelibrary.wiley.com/terms-and-conditions) on Wiley Online Library for rules of use; OA articles are governed by the applicable Creative Commons License

Author Manuscript

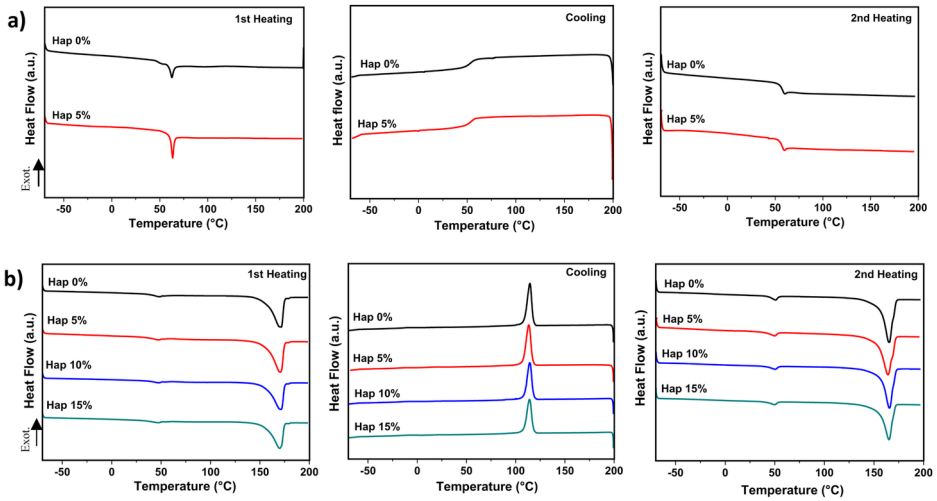


APP_50139_Figure 7.tif

This article is protected by copyright. All rights reserved.

10974628, 2021, 14, Downloaded from https://onlinelibrary.wiley.com/doi/10.1002/app.50139 by The University Of Texas Rio Grande Valley, Wiley Online Library on [19/12/2022]. See the Terms and Conditions (https://onlinelibrary.wiley.com/terms-and-conditions) on Wiley Online Library for rules of use; OA articles are governed by the applicable Creative Commons License

Author Manuscript

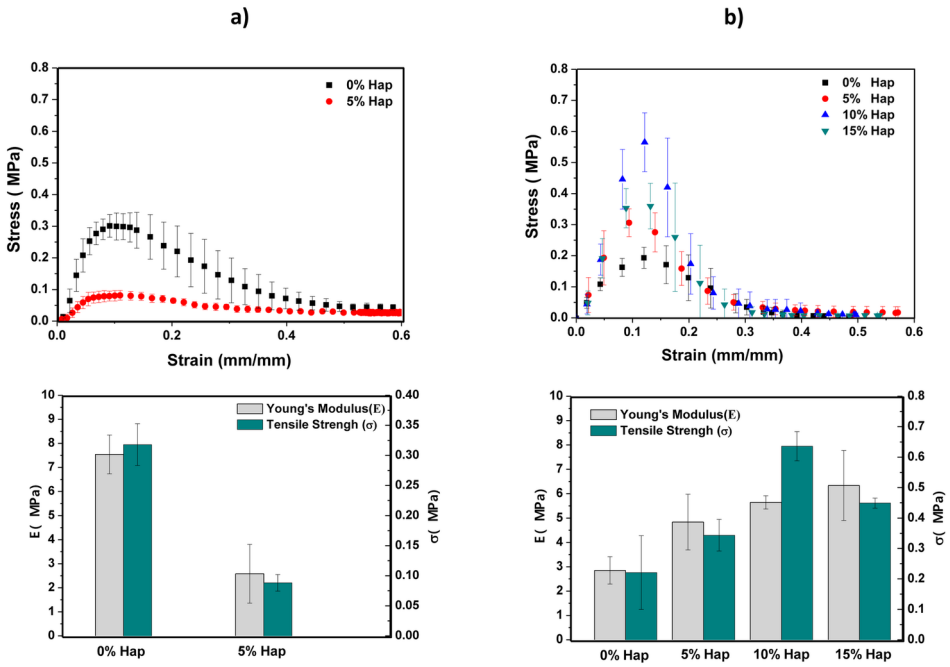


APP_50139_Figure 8.tif

This article is protected by copyright. All rights reserved.

10974628, 2021, 14, Downloaded from https://onlinelibrary.wiley.com/doi/10.1002/app.50139 by The University Of Texas Rio Grande Valley, Wiley Online Library on [19/12/2022]. See the Terms and Conditions (https://onlinelibrary.wiley.com/terms-and-conditions) on Wiley Online Library for rules of use; OA articles are governed by the applicable Creative Commons License

Author Manuscript

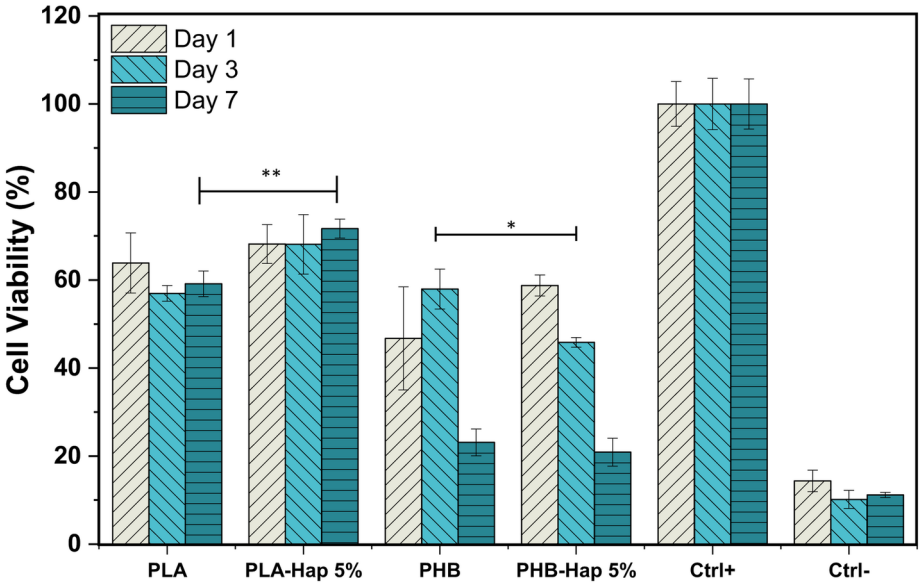


APP_50139_Figure 9.tif

This article is protected by copyright. All rights reserved.

10974628, 2021, 14, Downloaded from https://onlinelibrary.wiley.com/doi/10.1002/app.50139 by The University Of Texas Rio Grande Valley, Wiley Online Library on [19/12/2022]. See the Terms and Conditions (https://onlinelibrary.wiley.com/terms-and-conditions) on Wiley Online Library for rules of use; OA articles are governed by the applicable Creative Commons License

Author Manuscript

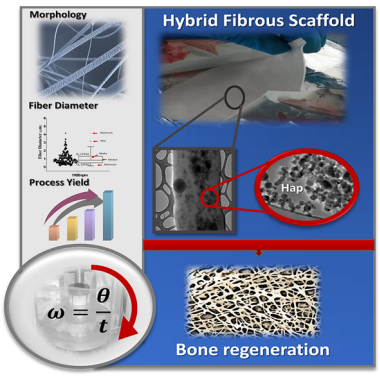


APP_50139_graphical abstract 10-14-20.tif

This article is protected by copyright. All rights reserved.

10974628, 2021, 14, Downloaded from https://onlinelibrary.wiley.com/doi/10.1002/app.50139 by The University Of Texas Rio Grande Valley, Wiley Online Library on [19/12/2022]. See the Terms and Conditions (https://onlinelibrary.wiley.com/terms-and-conditions) on Wiley Online Library for rules of use; OA articles are governed by the applicable Creative Commons License